A Geophysical and Field Survey in Central New Hampshire to Search for the Source Region of the Magnitude 6.5 Earthquake of 1638

Author: Justin C. Starr

Boston College

The Graduate School of Arts and Sciences

Department of Earth and Environmental Sciences

A GEOPHYSICAL AND FIELD SURVEY IN CENTRAL NEW HAMPSHIRE TO SEARCH FOR THE SOURCE REGION OF THE MAGNITUDE 6.5 EARTHQUAKE OF 1638

a thesis

by

JUSTIN C. STARR

Submitted in partial fulfillment of the requirements

For the degree of

Master of Science

August 2013

ABSTRACT

A GEOPHYSICAL AND FIELD SURVEY IN CENTRAL NEW HAMPSHIRE TO SEARCH FOR THE SOURCE REGION OF THE MAGNITUDE 6.5 EARTHQUAKE OF 1638

By Justin Starr

Advisor: Dr. John Ebel and Dr. Alan Kafka

In 1638, an earthquake with an estimated MLg of 6.5 ± 0.5 struck New England and adjacent southeastern Canada producing severe shaking in Boston, Massachusetts and Trois-Rivieres, Quebec. Previously published analyses of felt reports place the possible epicenter somewhere within a broad region including NY, NH, VT and ME. The possible source region had been further refined by the application of Omori's Law rate of aftershock decay combined with estimated rupture extent based on modern seismicity, which together suggest that a seismic event of MLg 6.5 ± 0.5 could have occurred in central New Hampshire in 1638. In order to more clearly define the possible active fault for this earthquake and determine its seismotectonic framework within central New Hampshire, three geophysical methods were used to analyze recent, digitally recorded seismic data. The three methods are a relative location analysis, computation of focal mechanisms and computation of focal depths based on fundamental mode Rayleigh waves. The combined results of the analyses are consistent with a thrust fault trending NNW - SSE and possibly dipping eastward in this postulated 1638 epicentral zone. Modern earthquakes in the postulated source area of the 1638 earthquake occur at focal depths of ~3 to 10 km with many of the events occurring ≥5 km, suggesting, that this is the depth range of the 1638 rupture. Depending on the depth of the pre-Silurian basement of the Central Maine Terrane, the source of the MLg 6.5 ± 0.5 earthquake of 1638 may be a basement-involved thrust fault or a reactivated east-dipping thrust fault

located between the nappes of the overlying Silurian-Devonian aged metasedimentary rocks. When the postulated fault plane is projected to the surface, portions of the Pemigewasset and Merrimack Rivers are found to flow within its surface expression, which suggests that the courses of these rivers may be fault controlled. A fourth research technique, a field survey, was undertaken to search for earthquake-induced liquefaction features along the Pemigewasset, Merrimack and Winnipesaukee Rivers as well as of the Suncook River Avulsion site. Several small strata-bound soft-sediment deformation structures were found during the survey. Although some of the features may be seismically induced, they may also have formed as the result of depositional processes and therefore cannot be attributed to the 1638 earthquake.

ACKNOWLEDGEMENTS

I would like to thank my adviser John Ebel for his guidance and support throughout the process of researching and writing my thesis. I would also like to thank Alan Kafka, Martitia Tuttle and Jesse Bonner for their willingness to help no matter how many times I bothered them with questions.

My appreciation and thanks goes out to fellow graduate students and staff in Devlin Hall and Weston Observatory for their support, camaraderie and the occasional distraction.

I am grateful to my family for their support and encouragement. Finally, I would like to thank Bonnie Bielec for being a pillar of strength in my life. Completing this thesis would not be possible without her constant support, love and encouragement.

TABLE OF CONTENTS

1. Introduction

1.1. Regional Geologic Setting

The study area of this thesis is located within the geologically complex Central Maine Terrane (CMT) (Bennett et al., 2006) (Fig. 1). The CMT extends from portions of southern New England, through New Hampshire and Maine, into New Brunswick. The bedrock within the study area is primarily composed Silurian-Devonian metasediments that were originally deposited into a deepwater depositional basin that closed in the Middle Devonian by the convergence of Laurentia and Avalon during the Acadian orogeny (Ludman et al., 1993). Various igneous plutons of the Devonian New Hampshire Plutonic Suite intrude upon the metasediment formations (Bennett et al., 2006). The major geologic structures of the CMT include the Bronson Hill Anticlinorium (BHA), the Kearsarge-Central Maine Synclinorium (KCMS), the Central New Hampshire Anticlinorium (CNHA) and the Lebanon Antiformal Synclinorium (LAS) (Eusden and Lyons, 1993). Within the study area, only the KCMS and the CNHA are visible (Fig. 1). The KCMS is located in the western portion of the survey region and is composed of a series of west verging nappes. Each nappe is bounded by a nappe-propagating thrust that dips east and is rooted in the CNHA. The CNHA is located in the eastern portion of the study area and acts as a "dorsal zone" which divides the west-verging nappes of the KCMS and the east verging nappes of the LAS.

The structures of the CMT are underlain by pre-Silurian basement**.** A décollement is inferred to lie between the CMT rocks and the underlying basement (Brown and Solar, 1999). The thickness of the CMT metasedimentary rocks above the décollement has been estimated to be as thin as 3 km by Eusden and Lyons (1993), but other estimates of the

thickness of the metasedimentary rocks range up to 10 km (Thompson et al., 1993; Stewart et al., 1993).

The surficial geology of the survey area largely reflects sediment deposition related to the most recent period of continental glaciation, known as the Wisconsinan (Franzi et al., 2008). The Wisconsinan ice sheet began its retreat from its maximum extent ~25 ka and eventually moving away from central New Hampshire ~12.5 ka (Ridge et al., 2001). As the ice sheet receded, large glacial lakes such as Glacial Lake Franklin, Merrimack and Hooksett formed in the river valleys of central New Hampshire, with many smaller lakes forming in the tributary valleys (Tinkham and Brooks, 2009; Franzi et al., 2008). These lakes formed as the ice sheet blocked north-draining rivers and deltas blocked drainage in larger valleys to the south. Meltwater from the ice sheet mobilized and sorted previously ice-bound sediments such that coarse grain sediments were deposited closer to the glacier margin and finer grain sediments were deposited downstream in the deeper water of the larger lakes. In the deeper water, alternating layers of lake-bottom silt and clay were deposited and contain evidence of seasonal variation in meltwater flows. Rebound of the continent allowed drainage networks to take their modern form as streams cut terraces through older glacial sediments and deposited alluvium in their floodplains in post-glacial times (Franzi et al., 2008).

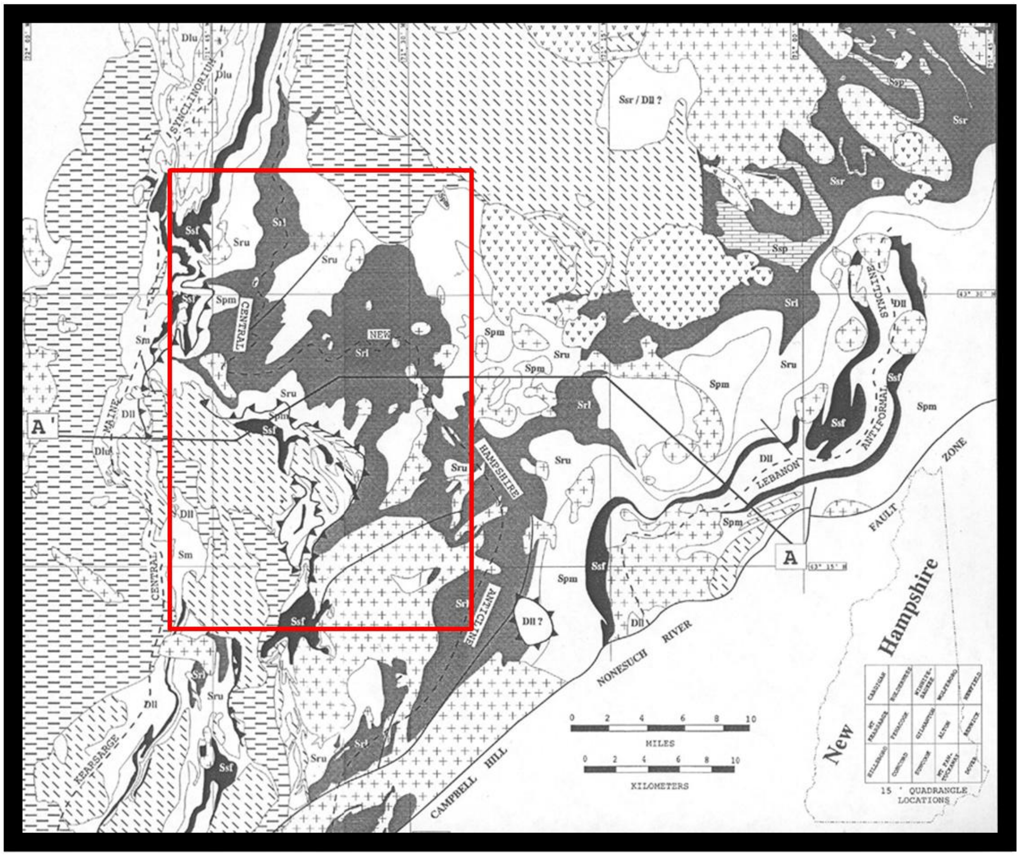
A'
A
Ssr / Dll ?
Ssr
Ssp
Srl
Sru
Ssf
Spm
Sm
Dll
Dlu
Dll ?
NEW
CENTRAL
HAMPSHIRE
ANTICLINE
MAINE
SYNCLINORIUM
KEARSARGE
LEBANON
ANTIFORMAL
NONESUCH RIVER
CAMPBELL HILL
FAULT
ZONE
New
Hampshire
MILES
KILOMETERS
15 ' QUADRANGLE LOCATIONS

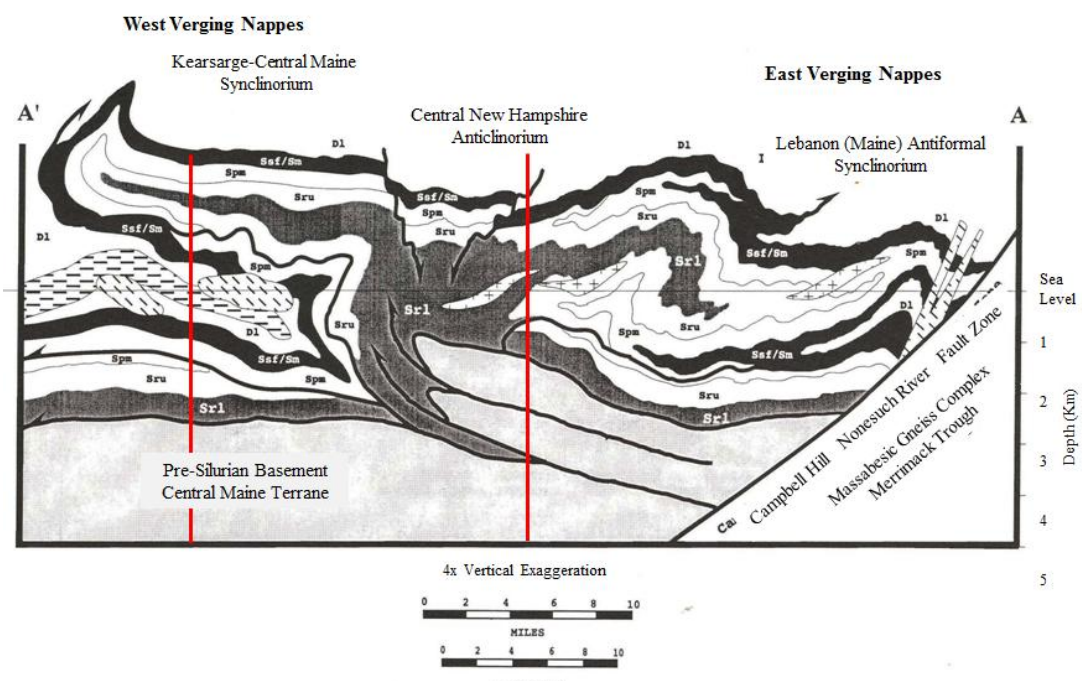
West Verging Nappes
Kearsarge-Central Maine Synclinorium
East Verging Nappes
Central New Hampshire Anticlinorium
Lebanon (Maine) Antiformal Synclinorium
A'
A
Dl
Ssf/Sm
Spm
Sru
Srl
Sea Level
1
2
3
4
5
Depth (Km)
Pre-Silurian Basement Central Maine Terrane
Campbell Hill Nonesuch River Fault Zone
Massabesic Gneiss Complex
Merrimack Trough
4x Vertical Exaggeration
MILES
KILOMETERS

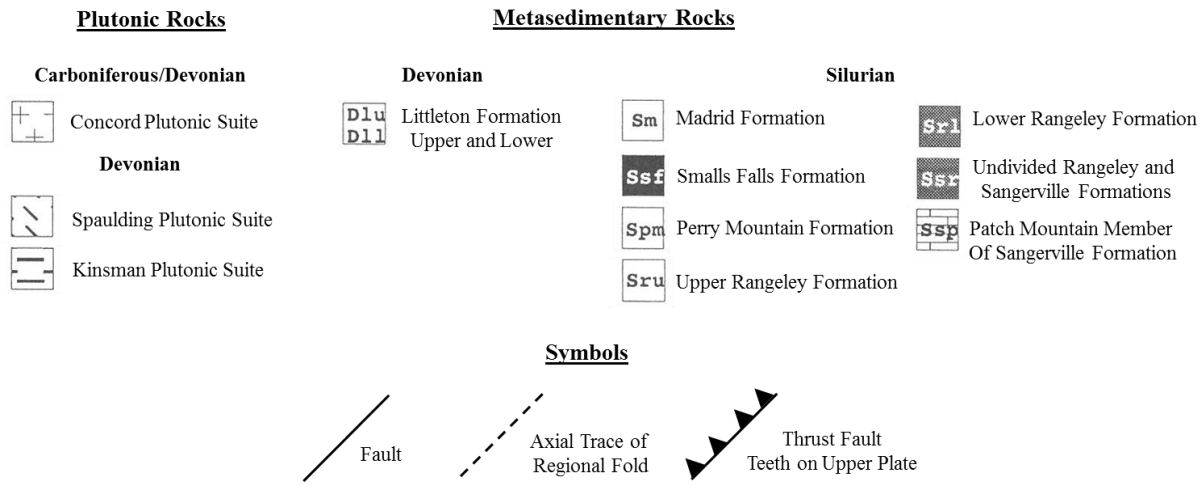

Figure 1: Geologic map and cross section through central-eastern New Hampshire from Eusden and Lyons (1993). The A' – A line transects through central New Hampshire. The red rectangle shows the approximate bounds of the study area of this thesis. The thin line indicating sea level is the approximate erosional level exposed today in central New Hampshire. Eusden and Lyons (1993) place the depth of pre-Silurian basement at 3 km but acknowledge that this depth is poorly constrained. Other estimates place the depth of the top of the pre-Silurian basement up as deep as 10 km (Thompson et al., 1993; Stewart et al., 1993).

1.2. Historical Accounts of the 1638 Earthquake

In 1638, the European settlement of New England was in its 18th year of existence. The Massachusetts Bay Colony and the town of Providence were rapidly growing while Jesuit missionaries moved north into Quebec with the intent of establishing churches and converting Native Americans in this region. Our ability to understand the occurrences of specific events that occurred within the New England colonies and in Quebec during the early colonial time period is due in large part to journal entries and private correspondence of those New England inhabitants and to the reports of Jesuit missionaries. By looking at these records today, we can find information about earthquakes that affected each colony and its inhabitants.

On June 1, 1638 of the Julian calendar (O.S), a strong earthquake struck New England. Jesuit missionaries at Trois-Rivieres along the St. Lawrence River in Quebec recorded water splashing out of kettles and bark dishes colliding against each other (Jesuit Relations, 1638). John Winthrop, the prominent governor of the Massachusetts Bay Colony, described in his journal how people in Plymouth had trouble standing during the earthquake shaking (Winthrop, 1908). William Bradford, writing *Of Plymouth Plantation*, describes how platters and dishes clattered and fell off shelves, that people had trouble standing and feared that their homes would fall (Bradford, 1952). Roger Williams, in writing to John Winthrop, describes feeling an earthquake but not as severe as that reported in Plymouth or in the Massachusetts Bay Colony (Winthrop, 1944).

1.3 Interpretations of the Location and Magnitude of the 1638 Earthquake

Although descriptions of the 1638 earthquake are consistent with a strong earthquake, the location and magnitude of the event have a wide uncertainty. To ascertain the magnitude of this earthquake, Ebel (1996) compared the intensity described at each location to the Modified Mercalli Intensity Scale (MMI) and used an intensity-magnitude-distance relation of Klimkiewicz (1982) to delimit the possible range of the location and size of the event. If the MMI at Trois-Rivieres and at Boston for the 1638 mainshock are both assumed to be VI, then Ebel (1996) argued that the earthquake could have had MLg 7.0 with an epicenter centered anywhere in central or northern Vermont or New Hampshire, northwest Maine or a small portion of northeastern New York (Fig. 2). A smaller magnitude would restrict the possible epicenter area roughly to central New Hampshire. Conversely, raising the Lg magnitude to 7.1 would move the eastern and western limits for the possible epicenter to eastern Maine or to the Lake Ontario region of New York, respectively (Fig. 2). Some aftershock activity was inferred from Winthrop's account, which suggests that ground shaking below intensity VI was felt in the aftershocks in eastern Massachusetts. Using Winthrop's account and assuming that site intensities as low as MMI II would have been noticed in Boston, Ebel (1996) estimated that aftershocks between M 4.3 and M 4.8 could have been felt in Boston and that if the 1638 earthquake generated a few aftershocks above M 4.0 within the first three weeks after the mainshock, then an epicenter in the southern part of central New Hampshire would result in most or all of those aftershocks being felt in Boston. Based on his analysis of written reports of the 1638 earthquake, Ebel (1996) estimated that the 1638 mainshock had an Lg magnitude of 6.5 ± 0.5 with an epicenter somewhere in the

seismically active part of central New Hampshire at the southern part of the shaded area in Fig. 2.

The Ebel (1996) hypothesis of an MLg 6.5 ± 0.5 earthquake occurring within central New Hampshire in 1638 is supported by the application of the Omori Law rate of aftershock decay combined with the Gutenberg-Richter recurrence relation to the seismicity of central New Hampshire (Ebel et al., 2000). Omori's Law describes the temporal decay of aftershocks with time while the Gutenberg-Richter relation describes the distribution of the rate of events as a function of magnitude. With the assumption that current, small earthquakes are aftershocks of strong earthquakes that occurred in the past, Ebel et al. (2000) determined that an earthquake ranging between MLg 6.9 and MLg 7.5 could have occurred in a North-South trending zone of seismicity in central New Hampshire (Fig. 3), referred to as the Central New Hampshire Seismic Zone (CNHSZ), approximately 129 to 395 years ago (Ebel et al., 2000).

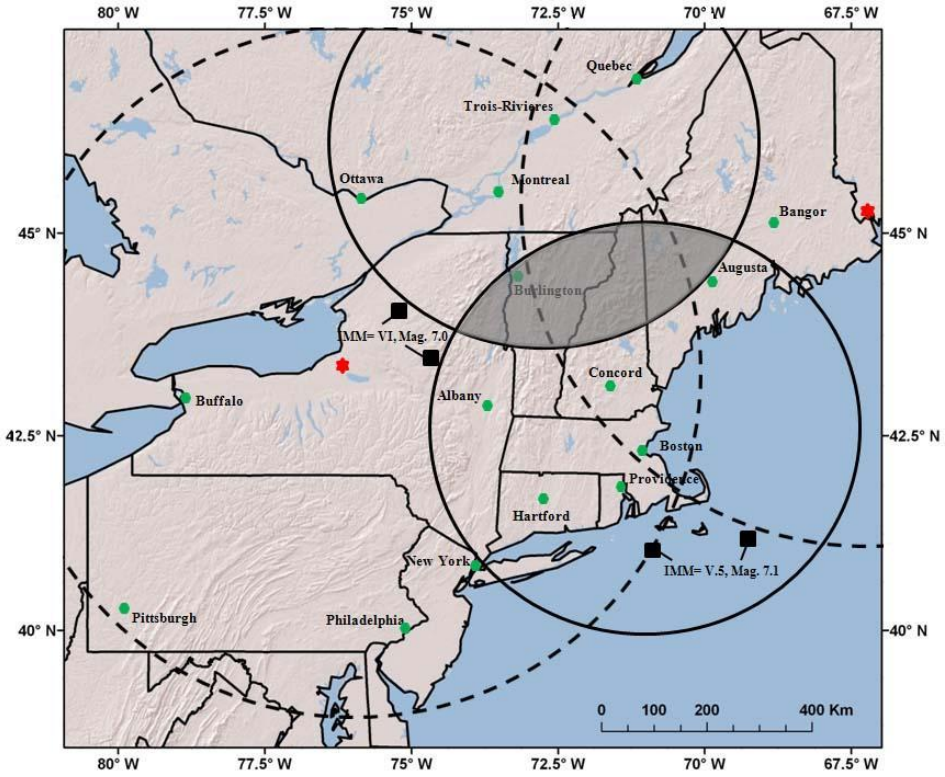

Figure 2: Map showing the area where the 1638 earthquake might have occurred (shaded area). The solid circles outline the MMI VI contours for a MLg 7.0 earthquake, centered on Boston and Trois-Rivieres. In addition, two stars indicate the easternmost and westernmost epicenter for a MLg 7.1 earthquake that would cause V ½ shaking at both Boston and Trois-Rivieres, shown by the dashed circles. Figure reproduced from Ebel (1996).

1.4 Hypothesis

The objective of this thesis is to determine the orientation of the postulated 1638 earthquake fault within the CNHSZ, determine where this fault may have a surficial expression, and determine if earthquake-induced liquefaction features that might have resulted from ground shaking during the 1638 earthquake can be found in the postulated epicentral region. To accomplish these goals, I computed high-resolution relative earthquake locations using recent, digitally recorded seismic data, provided an additional constraint of the focal depths of those recent earthquakes based on fundamental mode Rayleigh waves (Rg), determined event focal mechanisms and conducted a field survey to discover any possible surficial geologic evidence related to the 1638 earthquake.

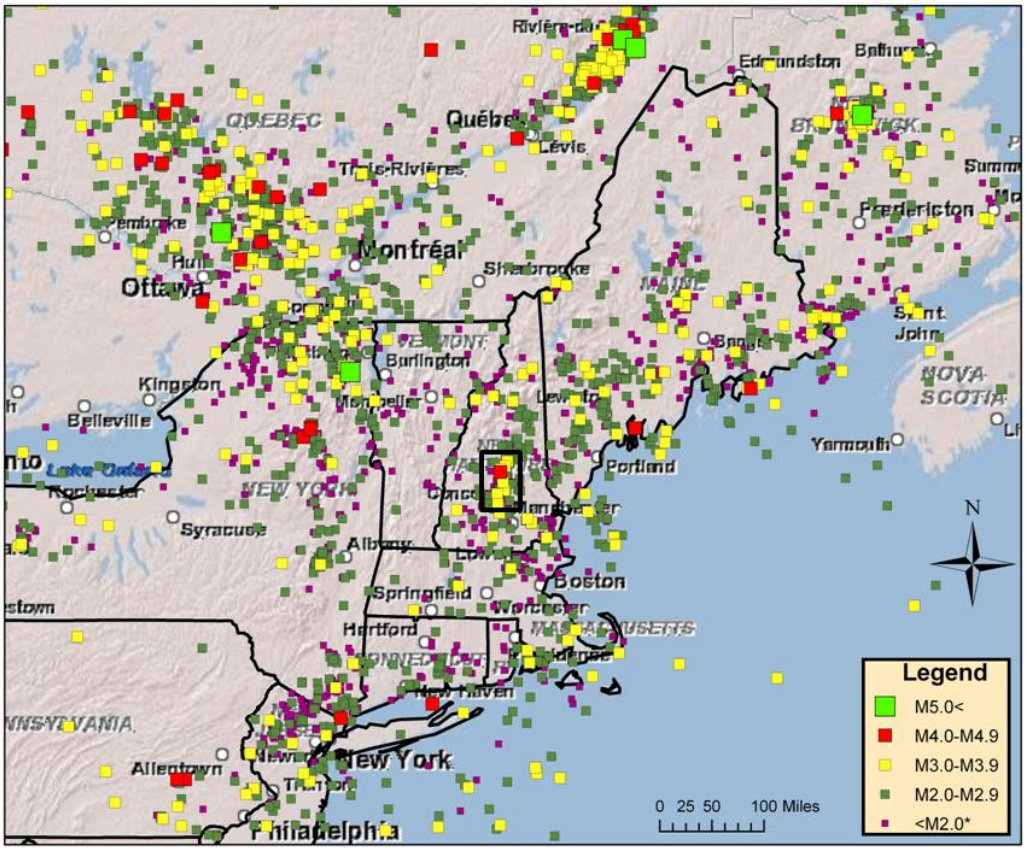

Figure 3: Seismicity map of the northeastern United States and portions of southeastern Canada produced by Weston Observatory, from October 1975 - December 2011 (http://www.bc.edu/research/westonobservatory/). The black rectangle in New Hampshire indicates the possible source region of the 1638 earthquake.

2. Data

The primary source of the data utilized in this study is digitally recorded seismic waveforms from the New England Seismic Network (NESN). Operated by Weston Observatory of Boston College, the NESN monitors seismic activity in Massachusetts, New Hampshire, Rhode Island, Maine, Vermont and Connecticut. A detailed description of each stage of the history of the New England Seismic Network can be found in Macherides (2003). The timespan of seismicity selected for this study is 1990 to 2009 (Table 1; Fig. 4). This timespan can be subdivided into 3 different periods, 1990 – 1992, 1992 – 2000 and 2000 – 2009, based on changes in operation and instrumentation of the seismic stations of the NESN. This division is important for purposes of this study since differences in either network operation or instrumentation affect the data analyses that were carried out in this thesis. In the early 1990s, the NESN consisted of approximately 30 stations **(**Fig. 5; Ebel, 1992**)** that provided seismic coverage of the six New England states. Beginning in 1992 and continuing to the early 2000's, funding issues forced the closure of many stations of the NESN while at the same time the network went through a series of station upgrades. These upgrades resulted in the installation of a newer, digital seismic network where data telemetry was initially by dial-up telephone connections and later by continuous data transmission via the internet. One effect of this transition period in the 1990s is a shortage of seismic stations for earthquakes that occurred between 1992 and 2000. Today, the network consists of 14 broadband stations covering each of the New England states (Fig. 6; Ebel, 2010**).** Seismic data from the NESN was used for the relative earthquake location analysis, computation of event focal mechanisms and computation of event focal depth using Rg.

A second source of seismic data utilized in this study is from seismic stations LONY, PKME, LBNH and HRV of the United States National Seismic Network (USNSN) (Fig. 6) as well as from stations of the now-discontinued MIT seismic network (Fig. 5). The USNSN stations along with the NESN stations are a part of the Advanced National Seismic System (ANSS). The MIT network consisted of nine seismic stations located in Massachusetts and New Hampshire. These stations operated from the 1970s to the early 1990s before the network was closed (Doll, 1992). The analysis of relative earthquake locations, focal mechanisms and earthquake depth determination from Rg used seismic data from the USNSN stations in addition to the data from the NESN. The MIT network provided data in addition to that from the NESN for the analysis of the relative earthquake locations and focal mechanisms. The MIT seismic station data were not used for the earthquake depth determination using Rg waves since the individual station amplitude responses are not known.

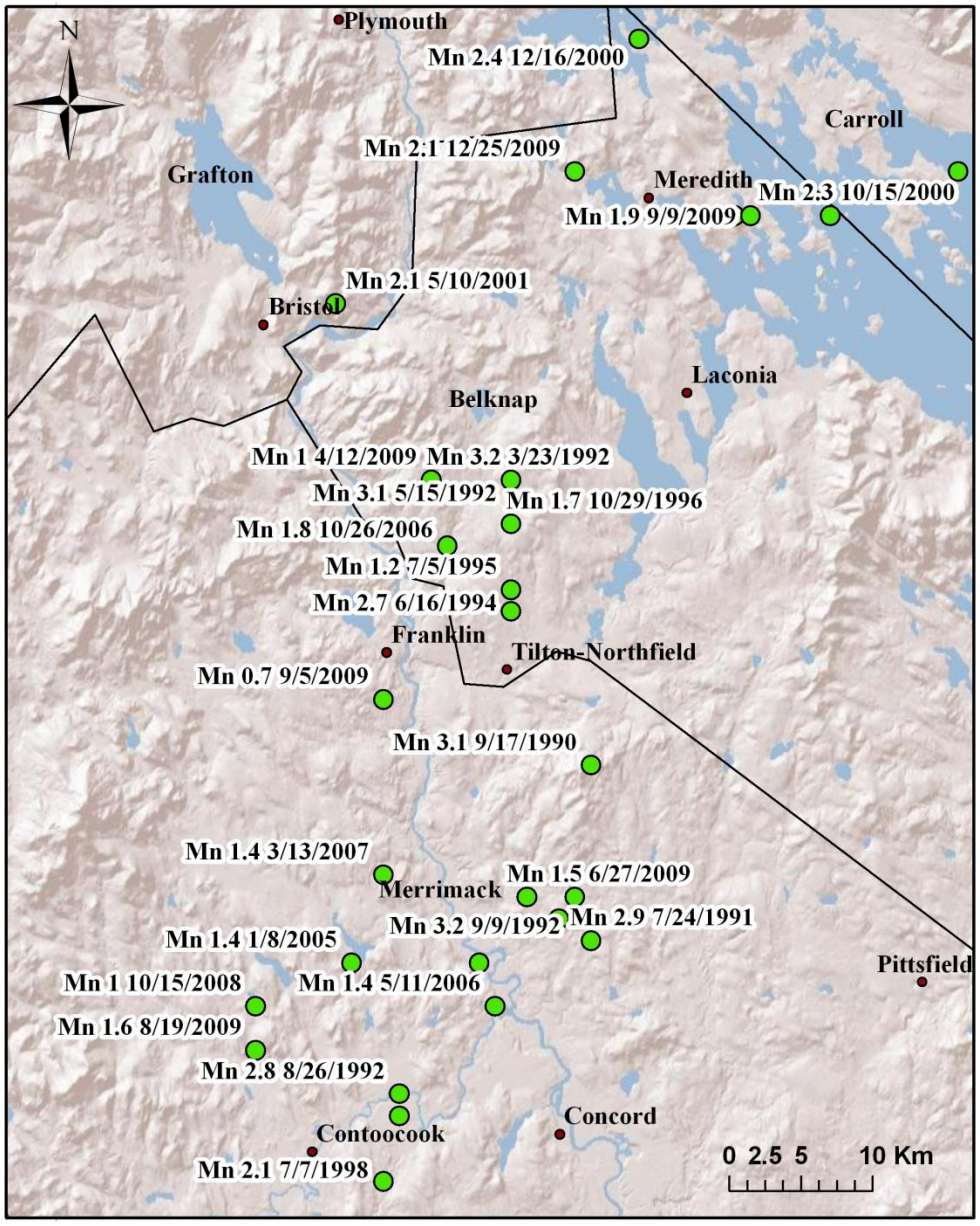

Figure 4: Map of each earthquake epicenter listed in Table 1 from the study area of this thesis. Black lines indicate the boundaries of the counties.

MM/DD/YYYY	HH:MM:SS.xx	-LAT-	-LON-	-DEP-	Mn	Mc	Remark
----------	----------	-----	-----	-----	---	---	----------
8/27/1990	06:39:11.38	43.31	-71.61	7.93	2.6	2.7	5 KM NORTH OF CONCORD
9/17/1990	23:01:37.64	43.4	-71.54	7.25	3.1	2.5	PITTSFIELD
7/24/1991	03:33:21.01	43.32	-71.54	9.26	2.9	2.8	10 KM SOUTH OF CONCORD
3/23/1992	10:01:50.46	43.53	-71.64	4.23	3.2	2.7	FRANKLIN
5/15/1992	20:34:35.78	43.53	-71.59	1.38	3.1	2.5	LACONIA
8/26/1992	23:04:48.94	43.25	-71.66	7.58	2.8	2.4	SW OF CONCORD
9/9/1992	19:00:51.78	43.34	-71.55	6.3	3.2	2.5	FRANKLIN AREA
10/6/1992	15:38:05.46	43.33	-71.56	2.76	3.4	3	FRANKLIN AREA
10/6/1992	17:05:49.73	43.33	-71.54	3.81	2.9	2.4	FRANKLIN AREA
6/16/1994	15:17:15.52	43.47	-71.59	1.49	2.7		SANBORNTON
7/5/1995	14:41:58.70	43.48	-71.59	5	1.2	1.9	TILTON
10/29/1996	17:50:21.75	43.51	-71.59	11.54	1.7	1.9	SANBORNTON
12/12/1996	19:13:42.65	43.67	-71.31	12.32	2.5	2.5	W OF WOLFEBORO
7/7/1998	09:41:42.44	43.21	-71.67	0.17	2.1		W of Concord
12/10/1999	01:08:51.75	43.24	-71.66	8.84	2.1		8 KM W OF CONCORD
10/15/2000	23:49:33.03	43.65	-71.39	1.05	2.3		10 KM E OF MERIDETH
12/16/2000	06:05:09.13	43.73	-71.51	10.24	2.4		CENTER HARBOR REGION
1/3/2001	23:05:29.51	43.65	-71.45	20.71	1.6		4 KM E OF MEREDITH
5/10/2001	16:27:11.91	43.61	-71.7	14.25	2.1		3 KM E OF BRISTOL
1/8/2005	20:30:00.92	43.31	-71.69	8.89	1.4		16 KM NW OF CONCORD
5/11/2006	22:37:26.91	43.29	-71.6	9.6	1.4	1.8	10.5 KM NW OF CONCORD
10/26/2006	13:03:03.61	43.5	-71.63	7.15	1.8	2	5.8 KM NNE OF FRANKLIN
3/13/2007	05:21:55.51	43.35	-71.67	3.16	1.4	2	10 KM SSW OF FRANKLIN
10/15/2008	07:39:12.48	43.29	-71.75	6.16	1	1.9	3.9KM NNW OF DAVISVILLE
4/12/2009	12:16:14.77	43.53	-71.64	5.73	1	1.8	9.5 KM N OF FRANKLIN
6/27/2009	15:57:52.68	43.34	-71.58	8.65	1.5	1.9	11.4 KM S OF TILTON
8/19/2009	20:37:29.83	43.27	-71.75	1	1.6	2.4	5.6 KM NNW OF CONTOOCOOK
9/05/2009	11:37:35.01	43.43	-71.67	6.66	0.7	1.6	2.7 KM WSW OF FRANKLIN
9/09/2009	13:25:06.25	43.65	-71.44	13.16	1.9	2.1	14.0 KM NNE OF LACONIA
12/25/2009	20:36:38.27	43.67	-71.55	2.57	2.1	2.2	17.0 KM NNW OF LACONIA

Table 1: A list of earthquakes that occurred within the study region between 1990 and 2009.

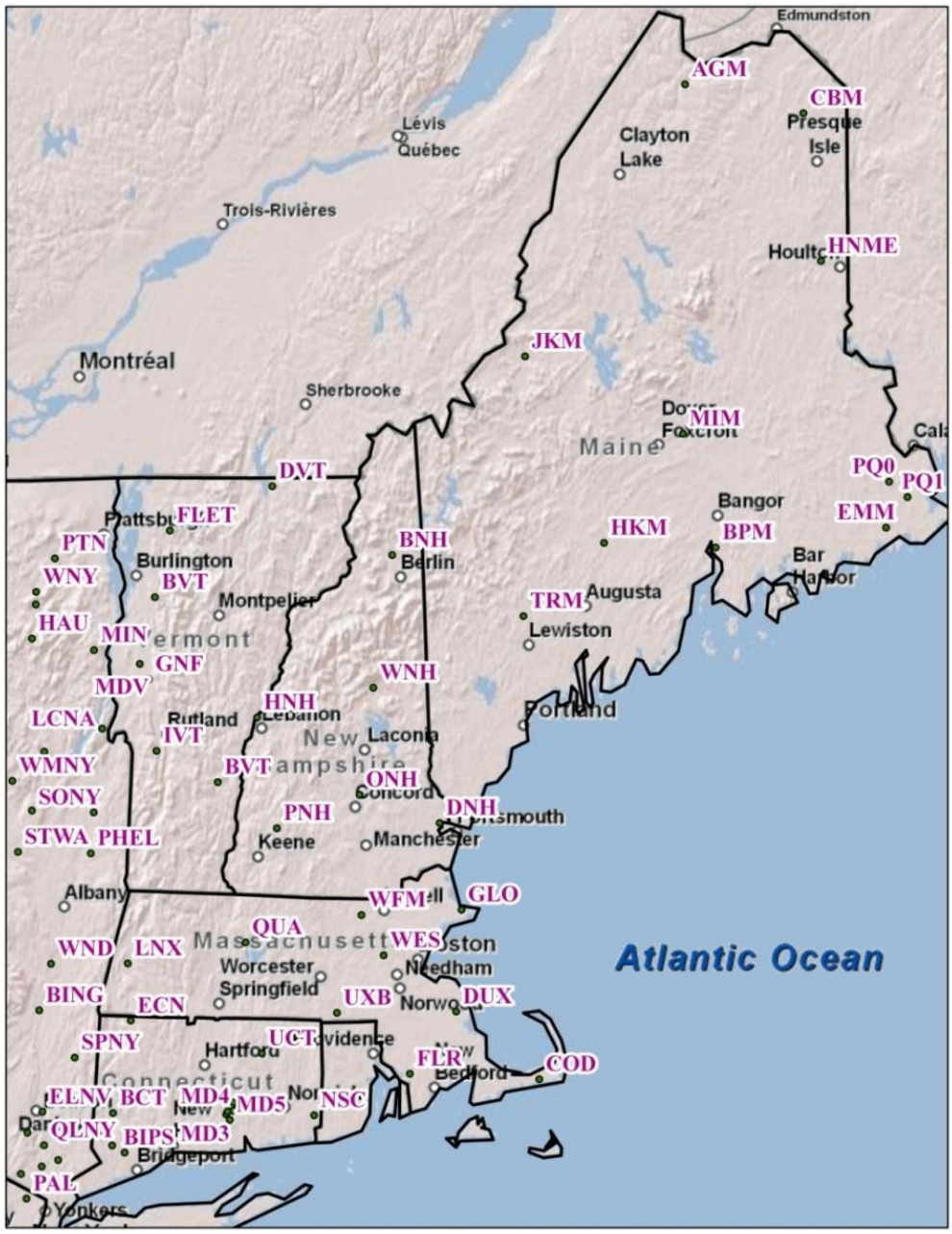

Figure 5: Locations of operational seismic stations in New England and eastern New York in 1990. Individual station information can be found in Ebel (1992).

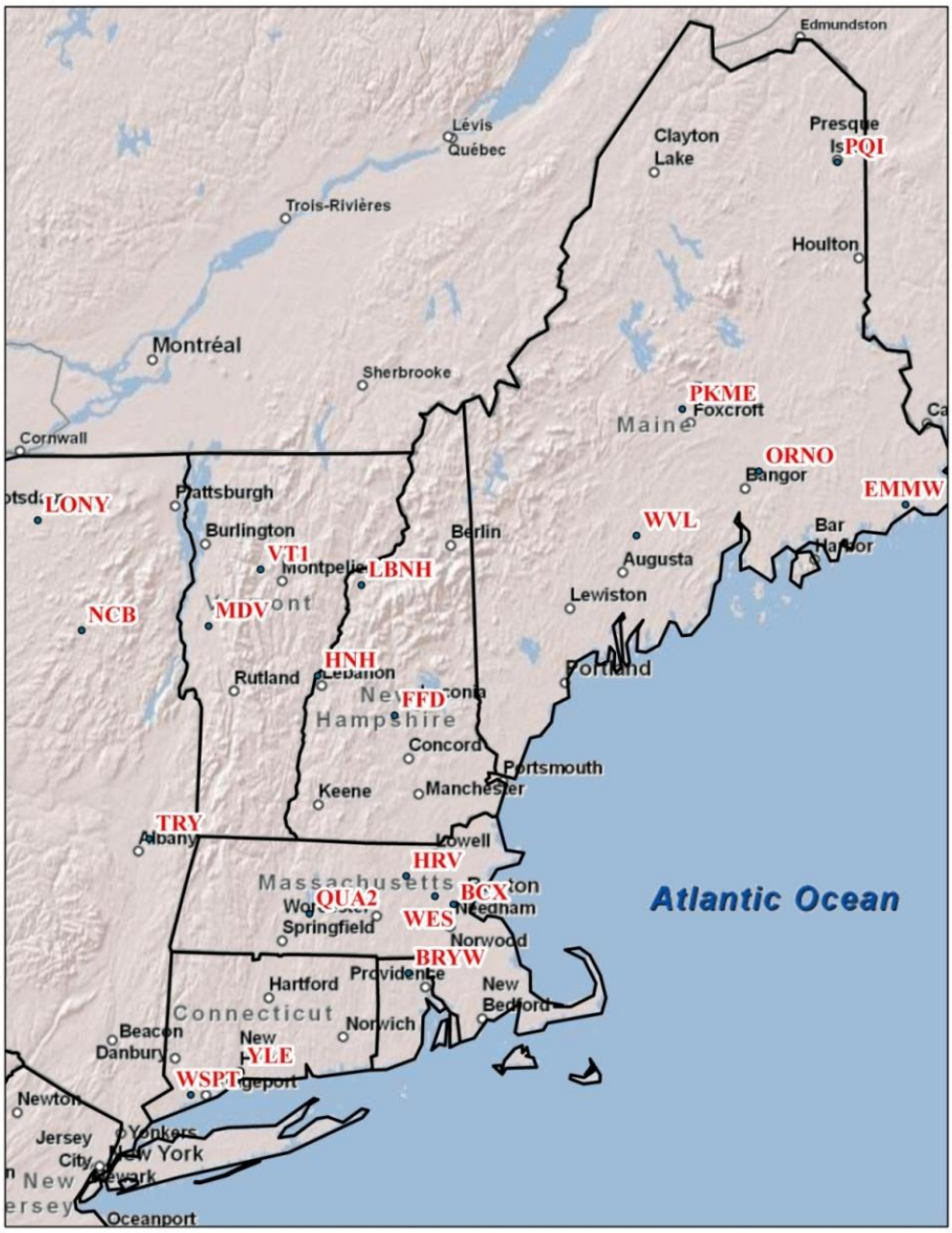

Figure 6: Distribution of seismic stations in the northeast United States at the time of this study. Individual station information can be found in Ebel (2010).

3. Relative Location Analysis

One of the reasons for monitoring earthquake activity in the CNHSZ, as well as northeastern North America in general, is to discover which geologic structures are seismically active. If seismically active structures can be found, they can be studied to decipher their past seismic history and to estimate their potential for large magnitude earthquakes. In general, the first step in monitoring seismicity in a region is to determine an absolute hypocenter for each earthquake. An absolute earthquake hypocenter is the set of absolute hypocentral parameters (latitude, longitude, depth and origin time) within a fixed, geographic system and fixed time base. The computation of the absolute hypocenter depends only on the observed P and S arrival times for the earthquake and on seismic velocities used in the location algorithm and is independent of the locations of all other earthquakes. Limitations on the accuracy of absolute hypocentral locations are controlled by several factors, including the network geometry, arrival-time reading accuracy, and knowledge of the crustal structure used in determining the hypocenter (Pavlis, 1986; Gomberg et al., 1990; Ellsworth and Roecker, 1981). For most earthquakes in the CNHSZ as well as for the rest of New England, an average error of about ±4 km exists for the latitude and longitude components of the absolute location epicenters, and the average error in focal depth is even greater at ±7.5 km (Ebel and Kafka, 1991; Ebel personal communication). A relative earthquake location is an event location that is determined with respect to the location of another earthquake, which itself may have an uncertain absolute location. A relative location analysis does not reduce the absolute location error but instead describes the spatial relationship of one earthquake relative to another. Often relative earthquake locations can be determined with much smaller

latitude, longitude and depth uncertainties than the uncertainties in the absolute locations of the individual events (Waldhauser and Ellsworth, 2000). Ultimately, an accurate absolute hypocenter of each earthquake is desired, but knowing the relative locations of epicenters with high precision are also of great value in attempts to discern whether seismicity is delineating an active structure. Locations can be accurate but imprecise (scatter around an active fault) or precise but inaccurate (narrowly following a fault-like pattern, but displaced from the true fault). The relative location analysis might produce a precise but inaccurate distribution of seismicity, but any suggestion of lineation or otherwise understanding the spatial relationship of one earthquake relative to another may provide valuable insight into the active geologic structure where these earthquakes occurred.

The purpose of the relative location analysis in this thesis is to identify the extent of spatial offset between the two events with much higher precision than the absolute locations of the individual events. The computation of this spatial offset is based on the differences in the source-to-station travel times for the two events. Earthquakes produce similar waveforms and source-to-station travel times at a common station if their focal mechanisms are nearly identical and if their sources are located close enough to each other that signal scattering due to velocity heterogeneities along the ray paths is nearly identical for the seismic energy from each of the two sources. Any difference in the waveforms and source-to-station travel times arise when there is a spatial offset between the events. To improve the precision of the relative arrival time readings for two different events at a common station, a waveform cross-correlation method using a master event can be used. In the master event approach, an event with good Signal-To-Noise Ratio

(SNR), located within a cluster of events, is used as a reference event for nearby secondary events within that cluster to be cross-correlated with. The locations of the secondary events can then be determined relative to that of the master event once the relative travel times have been determined by the cross-correlation method.

Cross-correlation is a measure of the similarity of two waveforms as a function of a time shift. Values of cross-correlation are greater at time shifts where the two signals are more similar and lower at time shifts where the signals are less similar. The cross-correlation of two signals, **x(t)** and **y(t)**, is defined as

$$\boldsymbol{C(L) = \lim_{T \to \infty} \frac{1}{T} \int_{-T/2}^{T/2} x(t) y(t + L) dt} \qquad \textbf{(1)}$$

where **C(L)** is the cross correlation value as a function of the time shift, **L**, **x(t)** is the master event waveform and **y(t)** is the secondary event waveform that is shifted **L** units in time. The time shift for which **C(L)** is maximum is the time shift at which the two waveforms are most similar.

For this thesis, I use the waveform cross-correlation method with a master event for determining the relative arrival times between the master event and each secondary event in a local cluster of earthquakes. In this thesis, the CNHSZ was split into several subsections, with each subsection having a radius of ~10 km. All events in each particular section are categorized as a single cluster. An event spatially located near the center of each cluster is selected as the master event for that cluster. The other events in each cluster are classified as secondary events with respect to the master event for the relative

location analysis (Table 2). The size of each cluster is based on Ebel et al. (2008) where the maximum distance between the absolute epicenter of the master event and secondary events used in his analysis is ~10 km. In each cluster, I cross-correlated the P and S waves of each secondary earthquake with the P and S waves of the master event of that cluster for seismic stations where the station recorded the P and/or S waves of both events. In particular, I made time series of 2-5 seconds data windows around the P and S wave arrival times of both earthquakes as selected by the seismic analyst who originally located the earthquake, beginning 1 second prior to this original arrival-time pick. The seismic waveforms contained in these windows were then cross-correlated with each other. This process is illustrated in Figs. 7a-d. A cross-correlation coefficient of 0.5 was used as the cut-off for including a particular arrival-time difference in the analysis. This cut-off value for the cross-correlation coefficient is taken from Ebel et al. (2008). The arrival time differences between the master event and the secondary event at several stations, each of which had associated cross-correlation coefficients of ≥ 0.5, were used in the relative location algorithm.

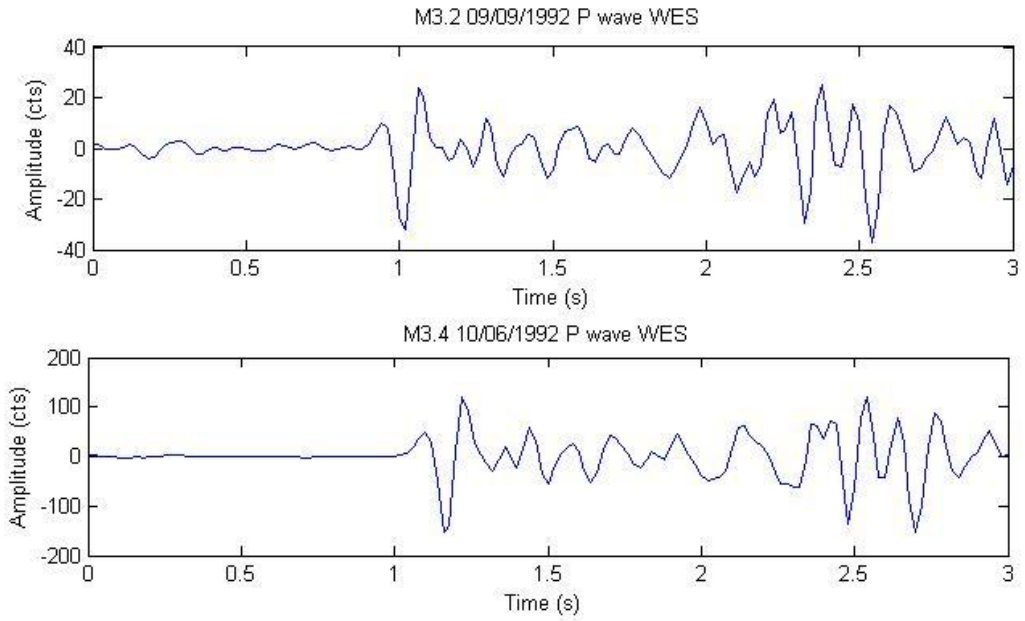

Figure 7a: The P-waves of the Mn 3.2 9/9/1992 and Mn 3.4 10/6/1992 earthquakes. The horizontal axis is in seconds. The vertical axis is in counts. The trace is positioned such that the analyst's pick occurs exactly 1 second into the displayed trace.

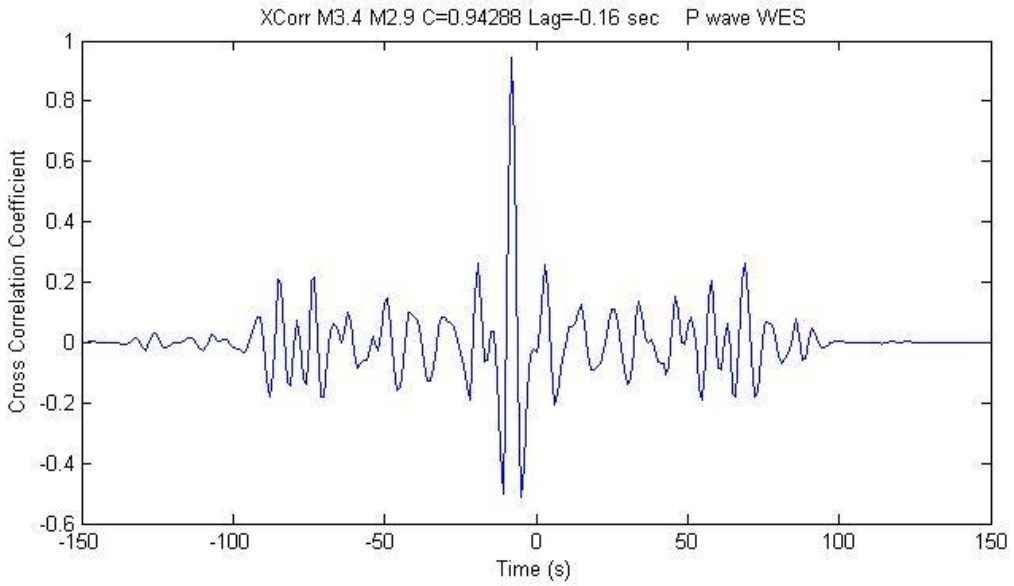

Figure 7b: The normalized cross correlation of the P-waves of Figure 7a. The header above the plot gives the maximum normalized cross correlation coefficient (C) and the relative time shift at the maximum correlation point (Lag).

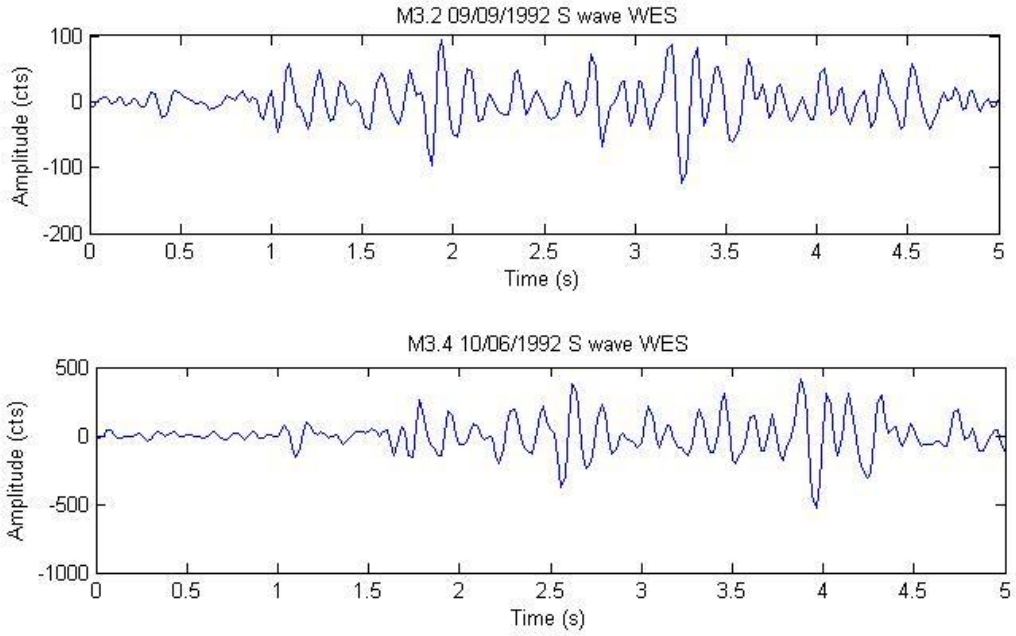

Figure 7c: The S-waves of the Mn 3.2 9/9/1992 and Mn 3.4 10/6/1992 earthquakes. The horizontal axis is in seconds. The vertical axis is in counts. The trace is positioned such that the analyst's pick occurs exactly 1 second into the displayed trace.

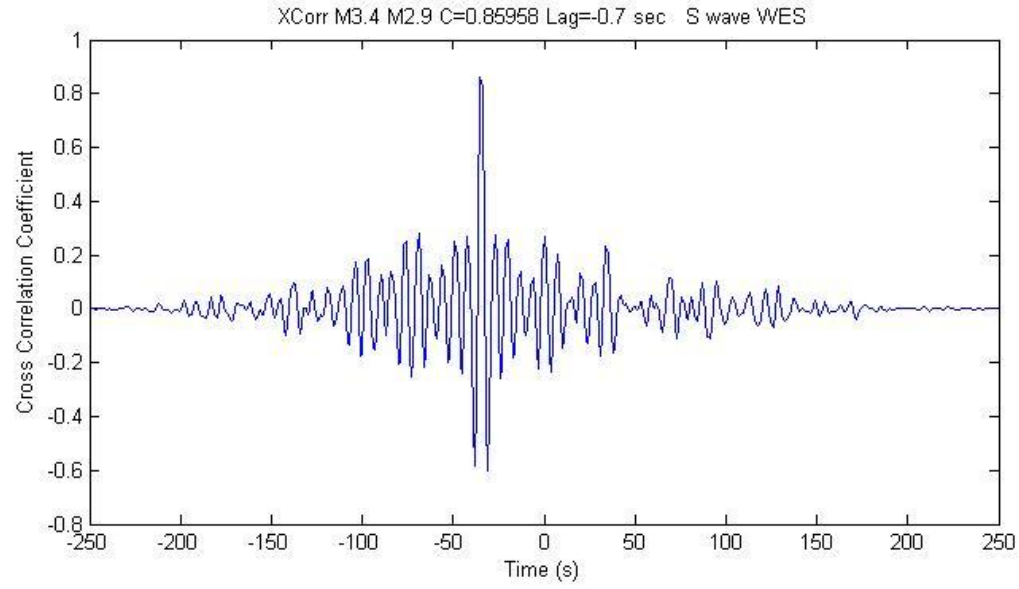

Figure 7d: The normalized cross correlation of the S-waves of Figure 7c. The header above the plot gives the maximum normalized cross correlation coefficient (C) and the relative time shift at the maximum correlation point (Lag).

3.1 Relative Location Algorithm

The relative location algorithm is based on the linear equation:

$$t_k^i - t_k^m = \frac{\partial t_k}{\partial x}\Delta x + \frac{\partial t_k}{\partial y}\Delta y + \frac{\partial t_k}{\partial z}\Delta z + \Delta\tau \qquad (2)$$

Where $t_k^i - t_k^m$ is the arrival time difference of the P or S phases between the master (*m*) event and the secondary (*i*) event for the *k* th phase. The partial derivatives in Equation (2) of the travel time *t* of a P or S wave for the master event with respect to the location coordinates (*x*, *y*, *z*) and the origin time (τ) are calculated for the ray path from the current hypocenter to the location of the station where the *k*th phase was recorded. Since the master and secondary events are close together spatially, the partial derivatives only need to use the seismic velocity structure near the hypocenter in their computation since the rest of the ray paths between the two earthquakes and the *i*th receiver should be quite common. The seismic velocity structure used in this thesis is the Hughes and Luetgert (1991) crustal model for central New Hampshire (Fig. 8). Δx, Δy, Δz and $\Delta\tau$ are the changes in the hypocentral location and origin time of the secondary event relative to the master event.

Equation (2) in matrix form can be written as:

$$\mathbf{Gm = d} \qquad (3)$$

where **G** is an M x 4 matrix containing the partial derivatives where M is the number of differential arrival time observations:

$$\boldsymbol{G} = \begin{bmatrix} \frac{\partial t_1}{\partial x}, & \frac{\partial t_1}{\partial y}, & \frac{\partial t_1}{\partial z}, & \mathbf{1}, \\ \vdots & \vdots & \vdots & \vdots \\ \frac{\partial t_k}{\partial x}, & \frac{\partial t_k}{\partial y}, & \frac{\partial t_k}{\partial z}, & \mathbf{1}, \end{bmatrix} \tag{4}$$

d is the M-length data vector containing the arrival time differences:

$$\boldsymbol{d} = \begin{bmatrix} t_1^i - t_1^m \\ \vdots \\ t_k^i - t_k^m \end{bmatrix} \tag{5}$$

m is the vector containing the changes in hypocentral parameters that the algorithm attempts to determine:

$$\boldsymbol{m} = \begin{bmatrix} \Delta x \\ \Delta y \\ \Delta z \\ \Delta \tau \end{bmatrix} \tag{6}$$

Equation (3) is solved by a least squares inversion:

$$\mathbf{G}^T \mathbf{G}\mathbf{m} = \mathbf{G}^T \mathbf{d} \tag{7}$$

where Equation (7) has the solution:

$$\mathbf{m} = (\mathbf{G}^T \mathbf{G})^{-1} \mathbf{G}^T \mathbf{d} \quad (8)$$

where **G**, **m** and **d** are defined in Equations 4-6.

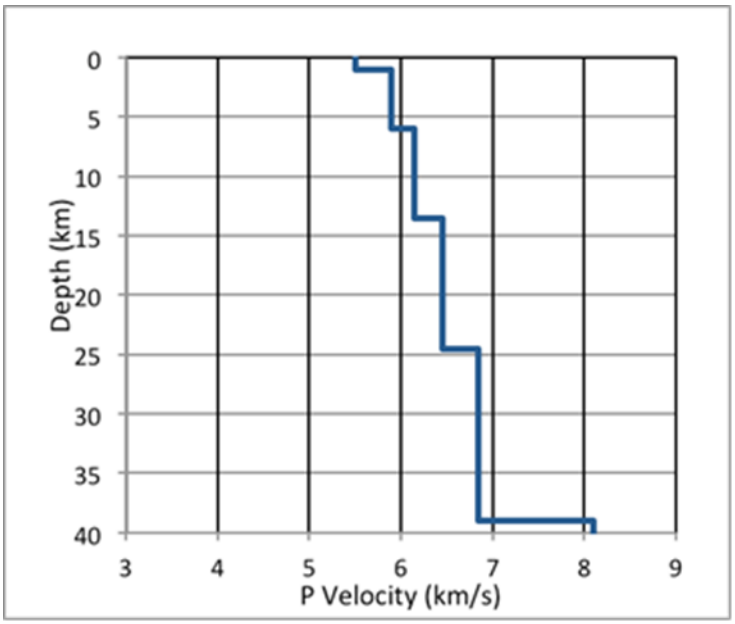

Figure 8: The Hughes and Luetgert crustal model for central New Hampshire (Hughes and Luetgert, 1991).

3.2 Relative Location Analysis Results

There are several requirements for computing accurate relative locations of two events. These requirements include the need for the secondary event to have at least 4 P or S differential travel time observations with the master event. Those differential travel-time observations were determined with cross correlation coefficients of ≥0.5 and where the common recording station locations for the master and secondary event are distributed around the CNHSZ and at a range of epicentral distances. Four earthquake clusters were selected for the relative location analysis (Table 2). Of the four clusters, only Cluster A satisfied the above requirements with four of its secondary events. Cluster A has an absolute location in the southern end of the study area, 19 km north of Concord NH (Fig. 9). The results of the relative location analysis are detailed in Table 3. Figure 10a-d shows the relative epicenters and focal depths of the secondary events relative to those of the Mn 3.2 09/09/1992 master event in map and cross-sectional views.

Cluster	Master Event	-LAT-	-LON-	Remark
A	Mn3.2 09/09/1992	43.34	-71.55	NH FRANKLIN AREA
B	Mn2.1 12/10/1999	43.24	-71.66	NH, 8 KM W OF CONCORD
C	Mn3.1 05/15/1992	43.53	-71.59	NH LACONIA
D	Mn2.1 09/09/2009	43.65	-71.44	14.0KM NNE OF LACONIA

Table 2: The master event and number of secondary events in each earthquake cluster.

A jackknife statistical analysis was carried out to estimate the uncertainty of the four hypocentral parameters of each relocated secondary event relative to the master event (Table 3). This statistical test involves omitting a single P or S differential travel-time observation and its associated derivatives from the relative location algorithm and

computing a new estimate of the event relative location. The algorithm is run several times omitting a single new data point each time until every point is omitted once. The result of each iteration is then used as a different sample estimate of the relative location from which the variance is computed. The relative location computed using all of the data is used as the expected value of the relative location in the variance computation.

Date	Mag (Mn)	dLat (km)	dLon (km)	dDepth (km)	dOT	RMS	Std. Dev of dLat	Std. Dev of dLon	Std. Dev of dDepth
8/27/1990	2.6	-4.01	-4.69	-3.19	744.5150	0.03	0.37	0.59	2.33
7/24/1991	2.9	-0.92	1.88	-0.87	413.6441	0.02	0.74	0.39	1.49
10/06/1992	2.9	-0.16	0.22	0.13	-26.9201	0.01	0.01	0.02	0.03
10/06/1992	3.4	-0.06	0.22	0.12	-26.8592	0.01	0.02	0.02	0.02

Table 3: The results of the relative location analysis and jackknife statistical analysis for Cluster A. Relative locations to the north, east and deeper are given by positive values. The root-mean-square (RMS) describes the error of each relative location. RMS values below the digital sampling period of the data (0.02 s) means that further resolution of the relative location is not possible. The digital sampling period of the data means that the location uncertainty cannot be reduced below about 120 m based on a hypocentral P-wave velocity of ~6.0 km/s, which is the average P-wave velocity for the upper 20 km of the crust in central New Hampshire.

The purpose of the relative location analysis using events of the CNHSZ and under the assumption that the recent events are aftershocks of the 1638 earthquake occurring on a common fault surface is to delineate the spatial relationship of one earthquake relative to another, thus providing insight into the possible orientation of the active geologic structure within the CNHSZ. The relative locations of the secondary events of Cluster A appear to follow a trend that is east-dipping (Fig. 10c-d). Thus, the depth distribution of these earthquakes is consistent with the fault of the 1638 earthquake dipping to the east.

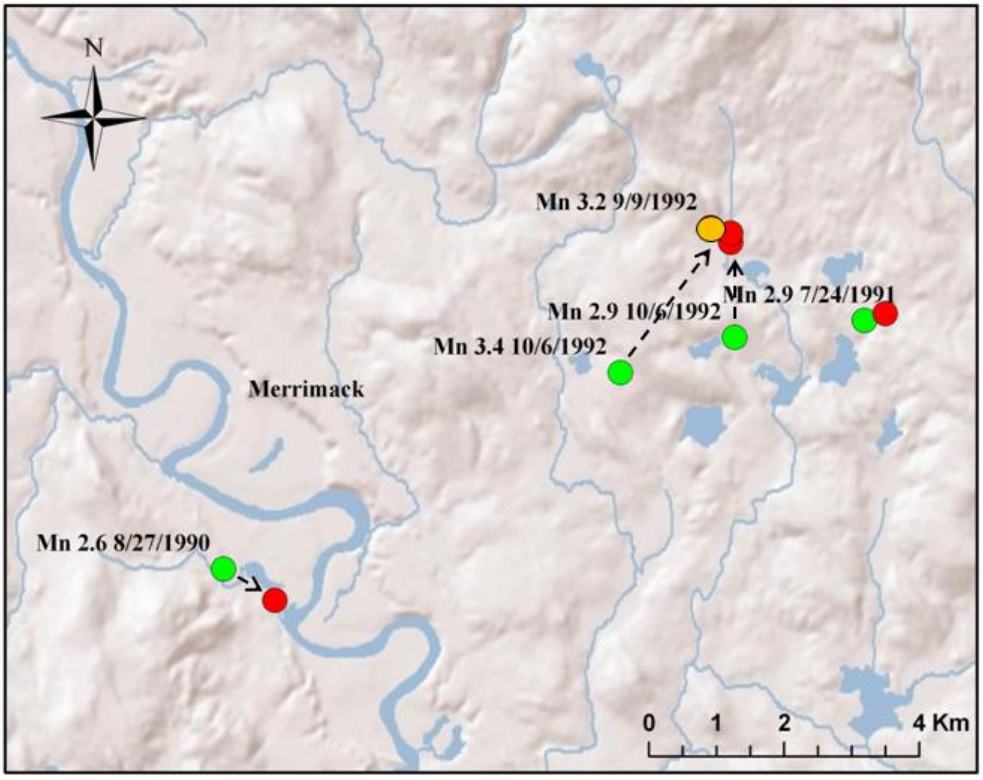

Figure 9: The earthquake epicenters of the master and the four secondary events of Cluster A. The orange dot is the absolute epicenter of the master event. The green dots are the original absolute epicenters of the secondary events. The red dots are the relative location epicenters of the secondary events relative to the absolute epicenter of the master event.

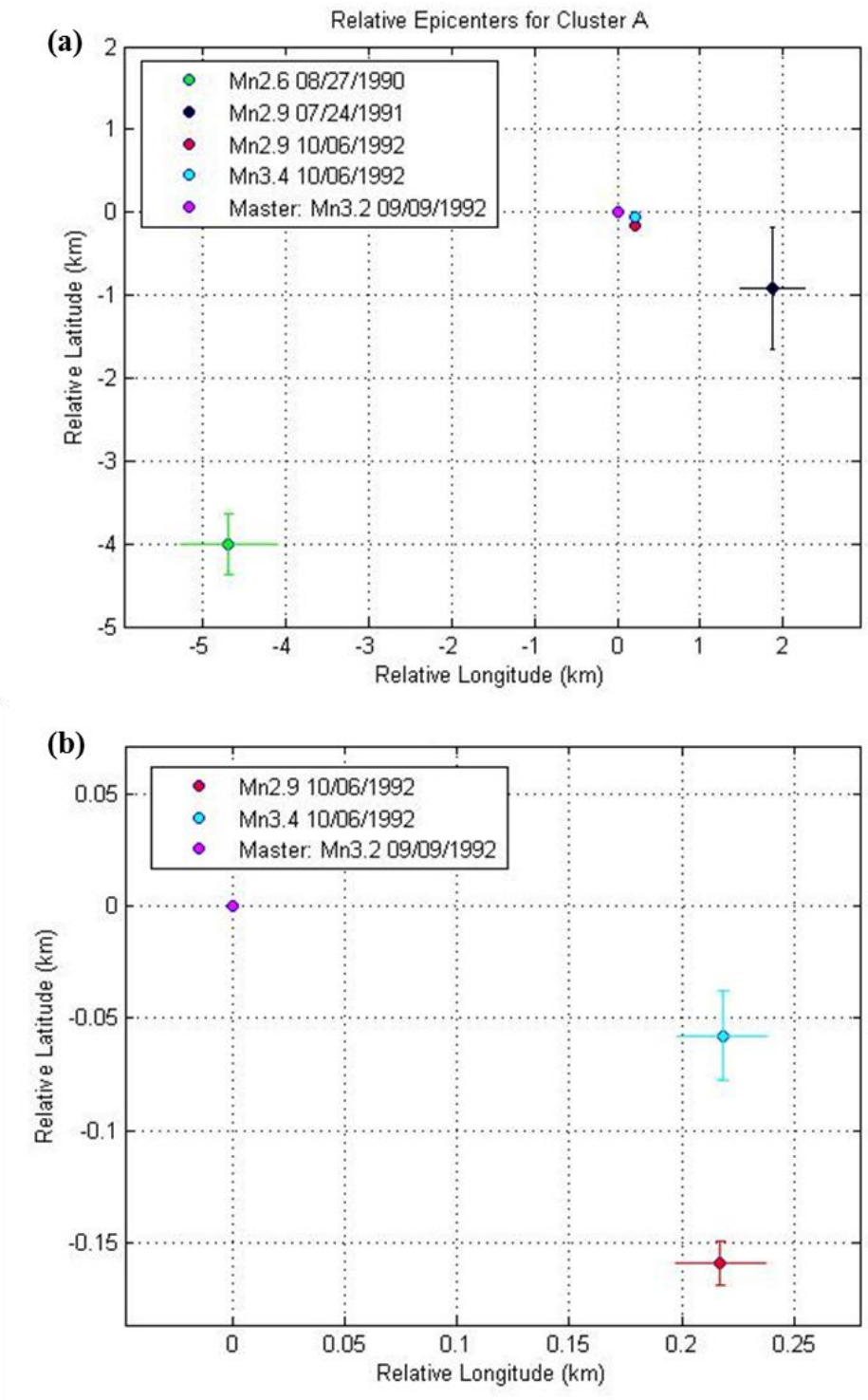

Figure 10: (a) The relative epicenters of the secondary events with respect to the Mn 3.2 9/9/1992 master event. **(b)** A close-up view of the epicenters of the Mn 2.9 10/6/1992 and Mn 3.2 9/9/1992 events relative to the master event.

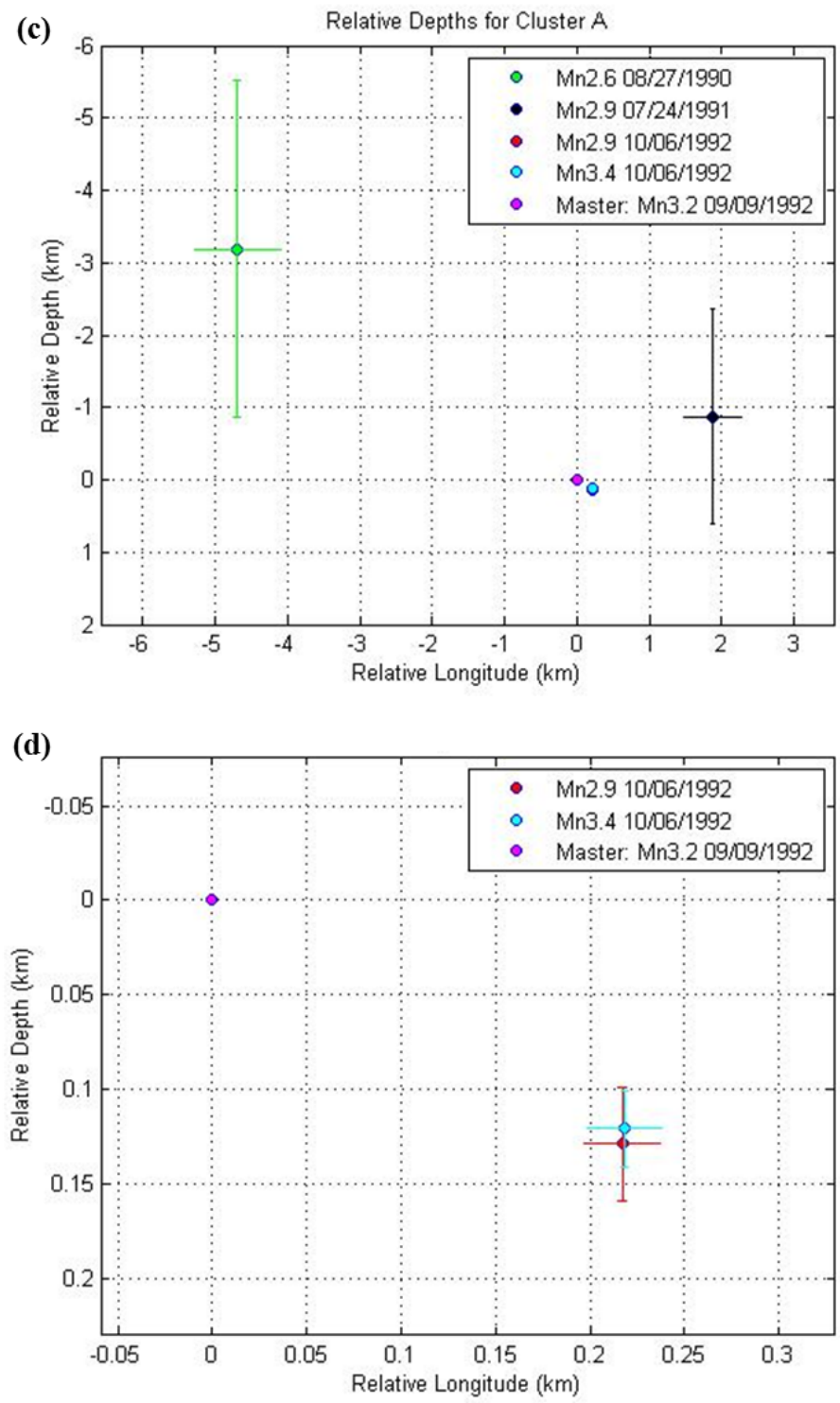

Figure 10 (Continued): (c) The relative depths of the secondary events with respect to the Mn 3.2 9/9/1992 master event. **(d)** A close-up view of the depths of the Mn 2.9 10/6/1992 and Mn 3.2 9/9/1992 events relative to the master event.

4. Focal Mechanism Solution

Focal mechanisms shed light on the geometry and nature of faulting in a seismic zone by determining the orientation of the possible fault plane and the direction of faulting on that plane for individual earthquakes. In this study, P-wave first motions are used to determine focal mechanisms for events within the CNHSZ. In particular, the P-wave first motions are read from digital data at all stations that recorded a particular event. The P-wave first motions that have clear, initial directions are analyzed with the program FOCMEC published by J. Arthur Snoke (Snoke, 2009). FOCMEC performs a grid search on the focal sphere for all possible focal mechanism solutions which fit the first motion data with the fewest number of inconsistent first motion readings.

In general, a fault plane solution with well-constrained nodal planes for a specific earthquake requires a sufficient quantity of first motion readings where the SNR for the initial P-wave is great enough that the initial P-wave polarity could be determined, at different azimuths. For New England, only those earthquakes larger than about Mn 3.0 satisfy this requirement. There are two reasons why New England earthquakes need to be larger than an Mn 3.0 to provide fault plane solutions with well-constrained nodal planes. First, there are not many seismic stations in this region, and so there are not many stations from which first motion readings can be made. Some of those stations have high background noise, reducing the probability that an unambiguous first motion can be read. The second reason is that most of the earthquakes have thrust focal mechanisms (Ebel and Bouck, 1988; Gephart and Forsyth, 1985; Pulli and Toksoz, 1981). Thus, many of the first arrivals at head-wave distances take off from near the nodal plane. This means that

the amplitude of the first arrival may be small, increasing the chances that the first arrival will be hidden in the background noise.

In April 1992, vertical-component station WNH of the now-discontinued MIT seismic network was reported to have a reversed polarity (Doll, 1992). Hypocenter documentation for the Mn 3.2 3/23/1992 event used in making the Ebel (1992) Quarterly Earthquake Report for New England, also described a reversed polarity for WNH. It is unknown when the station polarity became reversed and when (or if) the station hardware was changed to correct the polarity on the seismograms. For events for which a first motion was read at WNH and the polarity reversal was not explicitly described in the original earthquake documentation, two focal mechanism versions, one with a positive polarity at station WNH and one with a negative polarity at WNH, are computed. However, based on the station polarity information described Doll (1992) and Ebel (1992), the focal mechanisms with the reversed polarity at WNH are the preferred focal mechanisms.

4.1 Focal Mechanism Solution Results

Focal mechanisms were computed for several events within the CNHSZ. I read and selected the initial P-wave polarities for the Mn 3.1 9/17/1990 and Mn 3.2 3/23/1992 earthquakes and computed single-event focal mechanisms. In addition, based on the assumption from the relative location analysis that events that have accurate relative locations with each other have the same focal mechanism, I also computed a composite focal mechanism composed of P-wave polarity readings from events of Cluster A. The events of Cluster A are the Mn 3.2 09/09/1992, Mn 3.4 10/6/1992, Mn 2.9 10/6/1992, Mn 2.9 7/24/1991 and Mn 2.6 8/27/1990 earthquakes. The single-event focal-mechanism

solution for the Mn3.2 03/23/1992 event is shown in Figure 11. The original hypocenter documentation for this event published in Ebel (1992) assumed a reversed instrument polarity at WNH and stated that the initial P-wave first motion was dilatational for that station. Thus, since the ground motion at WNH is known, the focal mechanism shown here contains the published dilatation first motion at WNH for this event. This event focal mechanism suggests a thrust fault with some strike-slip motion with an E-W trending P-axis. Two possible focal mechanisms for the Mn 3.1 9/17/1990 event were computed (Fig. 12). If the WNH polarity reversal extends to September 1990, then the station has a dilatational first arrival and the focal mechanism for that event indicates a thrust fault with a N-S trending strike for both nodal planes and with the P-axis trending E-W (Fig. 12 Left). If WNH in September 1990 had normal polarity, then station WNH has a compressional P-wave first arrival and the focal mechanism is less well resolved with several different possible P, T and B axes (Fig. 12 Right).

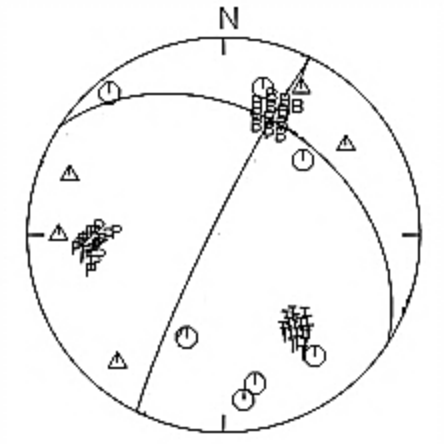

Figure 11: The fault plane solution for the Mn 3.2 3/23/1992 earthquake. The mechanism suggests primarily a thrust fault with some strike slip motion and an E-W trending P-axis. Hexagram indicates compressional first motion; triangle indicates dilatational first motion.

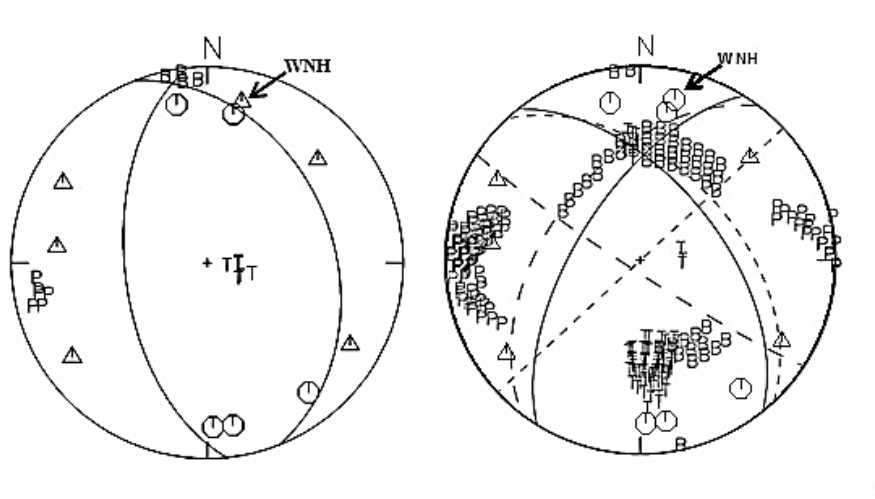

Figure 12: Two possible focal mechanism solutions for the Mn 3.1 9/17/1990 earthquake. (Left) The focal mechanism solution with WNH shown as a reversed polarity, dilatational first arrival. This suggests thrusting with a NNW-SSE trending strike fault and with a P-axis trending E-W. (Right) The focal mechanism with WNH shown as a correct polarity, compressional first arrival. This results in a poorly constrained fault plane solution with a wide range of possible P, T and B axis. An additional two pairs of nodal planes consistent with the data are shown, reflecting that wide range of P, T and B axis for the data set when the instrument polarity at WNH is not assumed to be reversed.

Two possible composite focal mechanisms were computed for the Mn 3.2 9/9/1992, Mn 3.4 10/6/1992, Mn 2.9 10/6/1992, Mn 2.9 7/24/1991 and Mn 2.6 8/27/1990 earthquakes (Fig. 13). If station WNH has a dilatational first arrival due to a reversed station polarity for all of these events, the composite focal mechanism describes a thrust fault with a NNW-SSE trending strike for both nodal planes with the P-axis trending E-W (Fig. 13 Left). If station WNH has a compressional first arrival due to an unreversed station polarity for all of these events, then the focal mechanism describes strike slip faulting with a P-axis trending E-W (Fig. 13 Right).

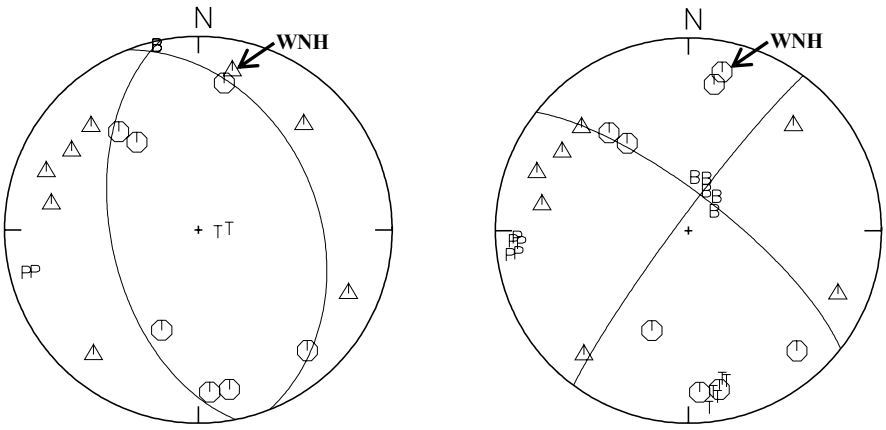

Figure 13: Two possible composite focal mechanisms for Cluster A. (Left) The composite focal mechanism with WNH shown as a reversed polarity, dilatational first arrival. This results in a thrust fault with a N-S trending strike with a P-axis trending E-W. (Right) The composite focal mechanism with WNH shown as a correct polarity, compressional first arrival that results in a strike-slip fault with a P-axis that trends E-W.

A general assumption of this thesis is that the current, small earthquakes occurring in the CNHSZ are aftershocks of the M6.5 1638 earthquake. Under this assumption, focal mechanisms computed for these modern earthquakes could serve as a surrogate focal mechanism for the 1638 earthquake. Thus, insight into the geometry and nature of faulting for the 1638 earthquake might be inferred from the single event focal mechanisms of the Mn 3.1 9/17/1990 and Mn 3.2 3/23/1992 events, the Cluster A composite focal mechanism and previously published focal mechanisms of the Mc 4.7 1/19/1982 earthquake at Gaza, NH, Mc 3.9 10/25/1986 earthquake near Northfield, NH and the Mc 3.1 6/28/1981 near Laconia, NH (Fig. 14; Ebel and Bouck, 1988). Even with the uncertainty in station polarity of WNH, the approximate E-W P-axis of the single event focal mechanism for the Mn 3.1 09/17/1990 event and of the Cluster A composite focal mechanism is consistent with that of the other single event focal mechanism for Mn 3.2 3/23/1992 event as well with the P-axis orientation of the previously published focal

mechanisms. Most of the focal mechanisms of the CNHSZ share a similarity in that they are purely thrust or at least have some component of thrust faulting. The only exception is the composite focal mechanism with WNH shown as a correct polarity, which shows pure strike-slip. However, based on the similarity of faulting style for the preferred focal mechanisms with the reversed polarity at WNH and of the previously published focal mechanisms along with the assumption that current, small earthquakes in the CNHSZ are aftershocks of the MLg 6.5 ± 0.5 earthquake of 1638, it is suggested in this thesis that the fault that produced the 1638 earthquake is a thrust fault with an approximate NNW-SSE strike. Using the results from the relative location analysis, the fault plane that is dipping to the east would be the preferred fault plane for the 1638 earthquake.

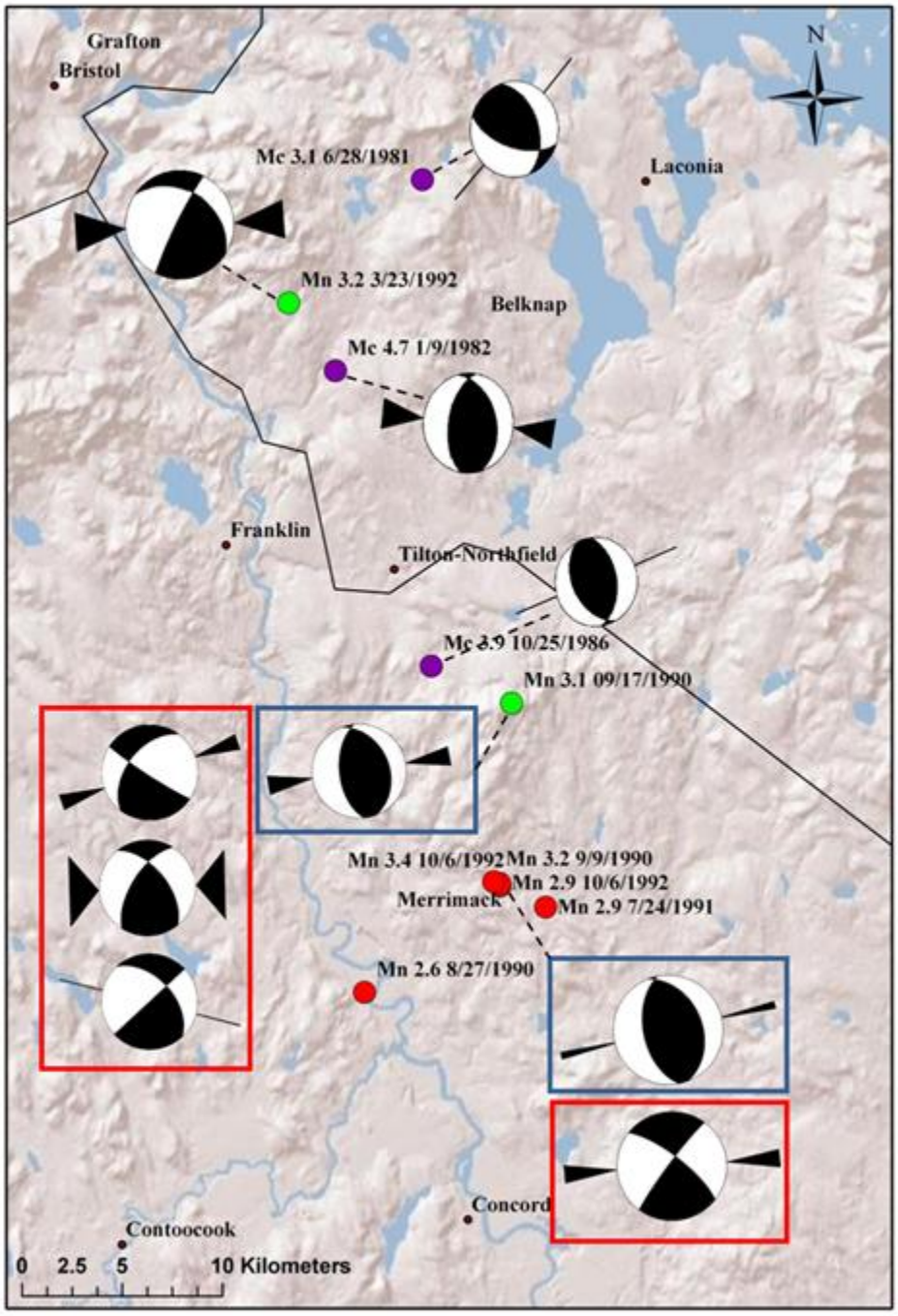

Figure 14: Map view of focal mechanism solutions for events in the CNHSZ. (Red Dots) The composite focal mechanism for Cluster A. (Purple Dots) Previous focal mechanisms computed for the CNHSZ. (Green Dots) The single event focal mechanisms computed in this thesis. (Blue Square) focal mechanism solutions with station WNH as a reversed polarity, dilatational first arrival. (Red Square) Focal mechanism solutions with station WNH as a correct polarity, compressional first arrival.

5. Focal Depth Estimation from Fundamental Mode Rayleigh Waves (Rg)

For a sparse seismic network, a trade-off exists between origin time and focal depth when computing hypocenters of seismic events using P and S arrival-time data (Gomberg et al., 1990; Ellsworth and Roecker, 1981). Since the regional seismic network in the northeastern U.S. is quite sparse in most areas, focal depths for almost all New England earthquakes are not very reliable because they suffer from this tradeoff. To estimate focal depths of the earthquakes in this thesis, independent of that from the hypocentral determination, the Kafka (1990) method of focal depth determination using fundamental mode Rayleigh waves (Rg) was utilized for the earthquakes in this study area.

5.1 Explanation and Identification of Rg and Lg Waves

The Kafka (1990) method involves the identification and analysis of two types of seismic waves. The first is a fundamental mode Rayleigh wave, known as Rg and first described by Press and Ewing (1952). An important characteristic of Rg waves is that they are dispersive. For dispersive signals, different wave packets arrive at different times, depending on their frequency. The Kafka (1990) method was developed based on well-studied Rg dispersion rates for a broadly defined region known as the Bronson-Avalon Dispersion Region (BADR), which covers Connecticut, Rhode Island and Massachusetts (Kafka 1988; Kafka and Dollin, 1985; McTigue, 1986). In the BADR, Rg group velocities have been determined for periods of approximately 0.5 s to 2.5 s (Fig. 15) which is a common Rg period range on seismograms of shallow focus earthquakes and explosions (Kafka, 1990). The Rg waves in the BADR have a group velocity

between 2.2 – 3.2 km/s (Table 4; Kafka, 1990). In that period range, most Rg energy is found on regional network seismograms for seismic sources within 2 or 3 km of the Earth's surface (Fig. 16). Focal depths deeper than 5 km do not generate strong Rg signals; thus, if Rg is clearly identified on a seismogram, the source is most likely within 5 km of the Earth's surface (Kafka, 1990, Kafka and Reiter, 1987). The second type of seismic wave utilized in the Kafka (1990) method is the Lg wave. Regional Lg is a guided wave, composed mainly of a sequence of multiply reflected post-critical S-waves trapped in a crustal wave-guide (Campillo, 1990; Bouchon, 1982). Kafka (1990) identifies the Lg wave train as having periods of 0.1 – 0.3 s and group velocities of 3.1 – 3.7 km/s (Table 4). Most New England earthquakes have a focal depth within 10 km of the surface (Ebel, 1985). The amplitude of Lg is fairly insensitive to source depth for events in this range (Shi et al., 2000; Campillo et al., 1984).

The key to the Kafka (1990) method is that the amplitudes of Rg waves are sensitive to source depth while Lg wave amplitude is generally not sensitive to source depth for crustal earthquakes. The determination of the ratio of the Rg energy to Lg energy from the seismogram at a seismic station can give a quantitative estimate of the focal depth of a seismic event independent of the absolute hypocentral determination from the P and S arrival time data.

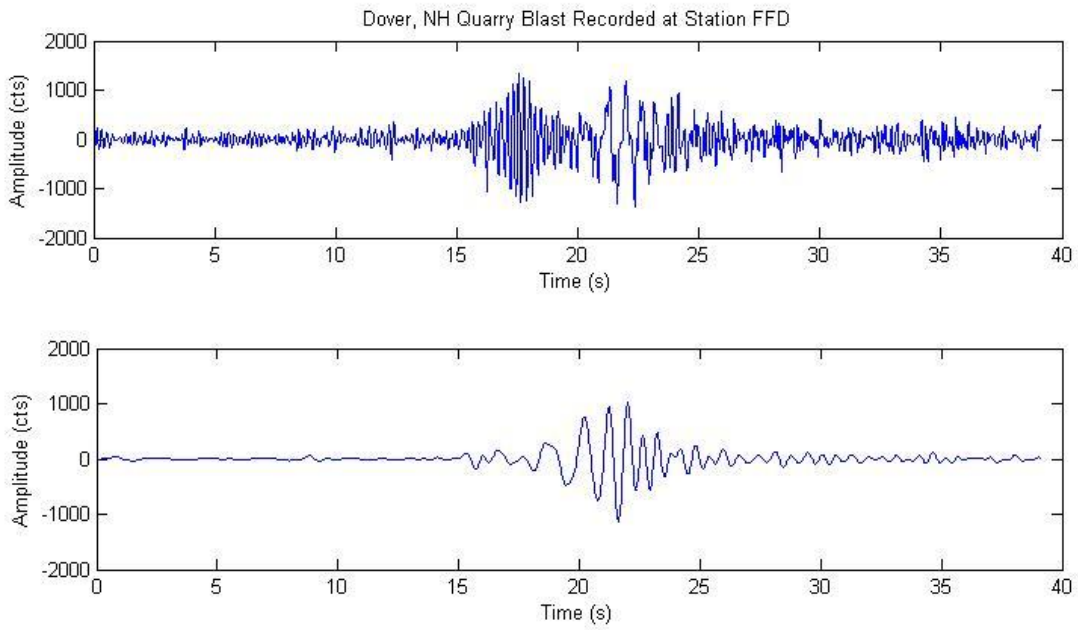

Figure 15: (Top) Seismogram of a quarry blast from Dover, NH that has a prominent Rg phase located between 18 and 24 seconds. The Lg phase exists between 15 – 18 seconds. (Bottom) A bandpass filtered seismogram of the Dover, NH quarry blast that highlights the Rg phase.

Group Velocity (km/s)						
4.0						
3.9						
3.8						
3.7	Lg	Lg				
3.6	Lg	Lg				
3.5	Lg	Lg				
3.4	Lg	Lg				
3.3	Lg	Lg				Rg
3.2	Lg	Lg				Rg
3.1	Lg	Lg		Rg	Rg	Rg
3.0				Rg	Rg	Rg
2.9			Rg	Rg	Rg	Rg
2.8			Rg	Rg	Rg	Rg
2.7			Rg	Rg	Rg	Rg
2.6			Rg	Rg	Rg	Rg
2.5			Rg	Rg	Rg	Rg
2.4			Rg	Rg	Rg	
2.3			Rg	Rg		
2.2			Rg			
2.1						
2.0						
	0.1	0.3	0.5	0.7	0.9	1.1

Period (s)

Table 4: Table of the expected arrival windows of Rg and Lg waves for a range of group velocities and periods. Table modified from Kafka (1990). The expected arrival window of Lg also includes expected arrival of the S-wave. Since S and Lg waves are difficult to separate at the distances and frequencies used in his analysis, Kafka (1990) defines the notation "Lg" to include the onset of the S-wave to the end of the S and Lg coda.

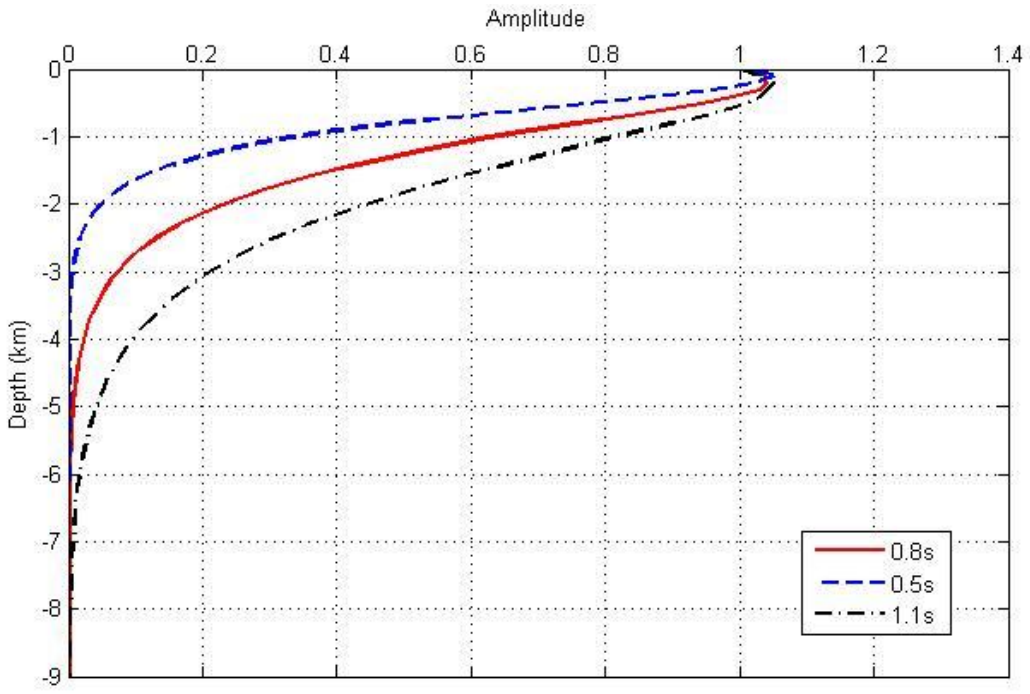

Figure 16: Details of the displacement-depth eigenfunctions for vertical Rg waves in central New Hampshire using the Hughes and Luetgert crustal model for central New Hampshire (Hughes and Luetgert, 1991). The 0.8 s eigenfunction was identified as representative of Rg in Kafka (1990) and is the eigenfunction used for analysis in this study. The eigenfunctions were computed using Computer Programs in Seismology by Robert Hermann of St. Louis University with a script provided by Jesse Bonner of Weston Geophysical Corp.

5.2 Similarity of Rg Dispersion in the BADR and the CNHSZ

An important aspect of applying the Kafka (1990) method to the CNHSZ is the similarity or dissimilarity of Rg dispersion between the BADR and CNHSZ. The Kafka (1990) method was developed based on well-studied Rg dispersion rates in the BADR. If Rg dispersion in the CNHSZ is different from that in the BADR, then in order to apply the Kafka (1990) method to the CNHSZ, several constants used in the Kafka (1990) computation need to be corrected for the differing Rg dispersion curves. Tu (1990) compared Rg dispersion in the BADR with other regions of New England, including the CNHSZ. Tu (1990) determined dispersion curves from explosion-generated Rg at two quarries, one in central New Hampshire and one in southern New Hampshire. These quarry blasts were recorded at stations in Vermont, New Hampshire and Massachusetts. When comparing the dispersion curves for explosion-generated Rg waves from New Hampshire to the dispersion curves of explosion-generated Rg waves from the BADR, Tu (1990) determined that the Rg dispersion curve of the CNHSZ lies within the same group velocity and period range as the BADR Rg dispersion curve with no significant difference between the two curves. Thus, the expected arrival window of Rg for the range of group velocities and periods shown in Table 4 can be applied to data from both the BADR and CNHSZ. Thus, no correction of the constants used in the formula of the Kafka (1990) method is necessary to apply his method to Rg data from the CNHSZ, given the similarity of Rg dispersion curves between the BADR and CNHSZ.

5.3 Multiple Filter Analysis

The Kafka (1990) method of utilizing Rg waves for depth determination begins by estimating the amount of Rg and Lg energy at different frequencies for a particular earthquake seismogram. This is achieved with the application of the Multiple Filter Technique (MFT) to the vertical component of that seismogram. Dziewonski et al. (1969) developed the MFT to provide an easy graphical assessment of multi-mode dispersive signals, which allows the determination of dispersion curves for the signals.

The mathematical form of the MFT as described by Dziewonski et al. (1969) begins with defining ω_n, the center frequency, and the window function written as

$$\boldsymbol{H_n(\omega) = e^{-\alpha \cdot \left(\frac{\omega-\omega_n}{\omega_n}\right)^2}} \qquad \textbf{(9)}$$

The inverse Fourier transform of $\mathbf{H_n(\omega)}$ is

$$\boldsymbol{h_n(t) = \frac{\sqrt{\pi} \cdot \omega_n}{2\alpha} \cdot e^{-\frac{\omega_n^2 \cdot t^2}{4\alpha}} \cdot \cos(\omega_n t)} \qquad \textbf{(10)}$$

The width of the $\mathbf{H_n(\omega)}$ window in the frequency domain is controlled by the parameter $\boldsymbol{\alpha}$ (Fig. 17).

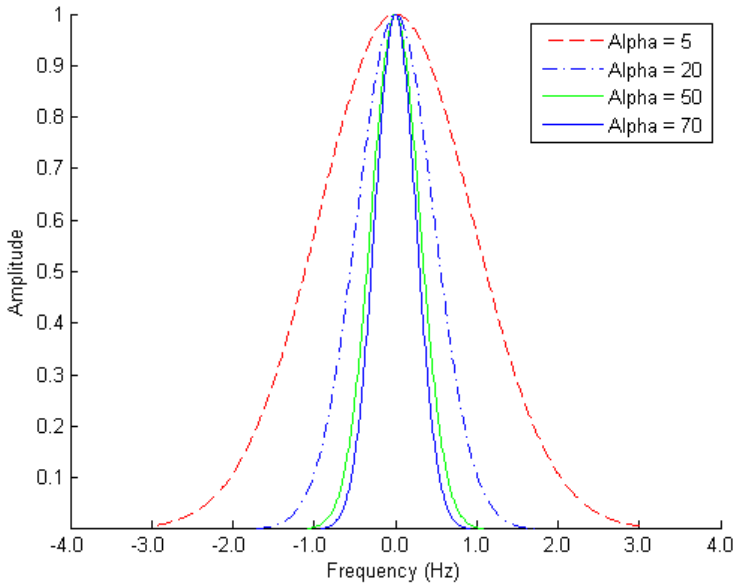

Figure 17: Multiple Filter (Gaussian function) using different values of α. Figure from Tu (1990).

The value of α used in this thesis is discussed below. The relative bandwidth of the filter is designated **BAND** where

$$\boldsymbol{BAND = 1 - \frac{\omega_{l\,n}}{\omega_n} = \frac{\omega_{u\,n}}{\omega_n} - 1} \qquad \textbf{(11)}$$

and the lower and upper band limits of the symmetrical filter, denoted as $\boldsymbol{\omega_{l,n}}$ and $\boldsymbol{\omega_{n,n}}$ respectively, are

$$\boldsymbol{\omega_{l\,n} = (1 - BAND) \cdot \omega_n} \qquad \textbf{(12a)}$$

$$\boldsymbol{\omega_{u\,n} = (1 + BAND) \cdot \omega_n} \qquad \textbf{(12b)}$$

The upper and lower band limits represent frequencies where the filter response is so low that anything outside that band is effectively cut out by the Gaussian filter. The parameter

β, which describes the decay of the filter, is determined by the desired value of the function at the band limits

$$\boldsymbol{\beta} = \ln[\frac{\boldsymbol{H_n(\omega_n)}}{\boldsymbol{H_n(\omega_{l\,n})}}] = \ln[\frac{\boldsymbol{H_n(\omega_n)}}{\boldsymbol{H_n(\omega_{u\,n})}}] \quad \textbf{(13)}$$

The parameter **α** of equations (9) and (10) can be expressed in terms of **BAND** and **β**

$$\boldsymbol{\alpha = \beta / BAND} \quad \textbf{(14)}$$

and the Gaussian window function is

$$\boldsymbol{H_n(\omega)} \quad \begin{cases} \mathbf{0} & ; \quad \boldsymbol{for\ \omega < (1 - BAND) \cdot \omega_n} \\ \boldsymbol{e^{-\alpha\left(\frac{\omega - \omega_n}{\omega_n}\right)}} & ; \boldsymbol{for\ (1 - BAND) \cdot \omega_n \quad \omega \leq (1 + BAND) \cdot \omega_n} \\ \mathbf{0} & ; \quad \boldsymbol{for\ \omega > (1 + BAND) \cdot \omega_n} \end{cases} \quad \textbf{(15)}$$

From Herrmann (2002), a dispersed surface-wave signal can be defined as

$$\boldsymbol{s(t) = \frac{1}{2\pi}\int_{-\infty}^{\infty} A(\omega) e^{i(\omega t - kx + \phi)}\, d\omega} \quad \textbf{(16)}$$

where $\boldsymbol{\phi}$ is the phase shift and **k** is the wavenumber. The filtered signal $\boldsymbol{g_i(t)}$, where $\boldsymbol{g_i(t)}$ is the filtered signal with the center frequency $\boldsymbol{\omega_i}$, results from multiplying **H(ω)** with the chosen frequency times the dispersed surface-wave signal in the frequency

domain and then completing an inverse Fourier transform of the signal to put it back into the time domain.

$$\boldsymbol{g_i(t) = \frac{1}{2\pi}\int_{-\infty}^{\infty} A(\omega)H(\omega)e^{i(\omega t - kx + \phi)}\, d\omega} \qquad \textbf{(17)}$$

The envelope, $\boldsymbol{a_n(t)}$ of the resulting function $\boldsymbol{g_i(t)}$ can be found by

$$\boldsymbol{a_n(t) = \sqrt{g^2(t) + y^2(t)}} \qquad \textbf{(18)}$$

where $\boldsymbol{y(t)}$ is the Hilbert Transform of the filtered trace (Fig. 18; Thrane, 1984).

The amplitude of the envelope at specific points, defined by the time where specific group velocities arrive at the recording station, is taken as the data for a dispersion plot. The process of recording the envelope amplitude values at specific points is repeated over a range of frequencies to produce the dispersion curve (Fig. 18). For this thesis, the frequency and group velocity ranges are 0.9 - 10 Hz (or periods of 0.1 s to 1.1 s) and 2.0 – 4.0 km/s, respectively (Table 4). This range contains the expected window of both Rg and Lg waves.

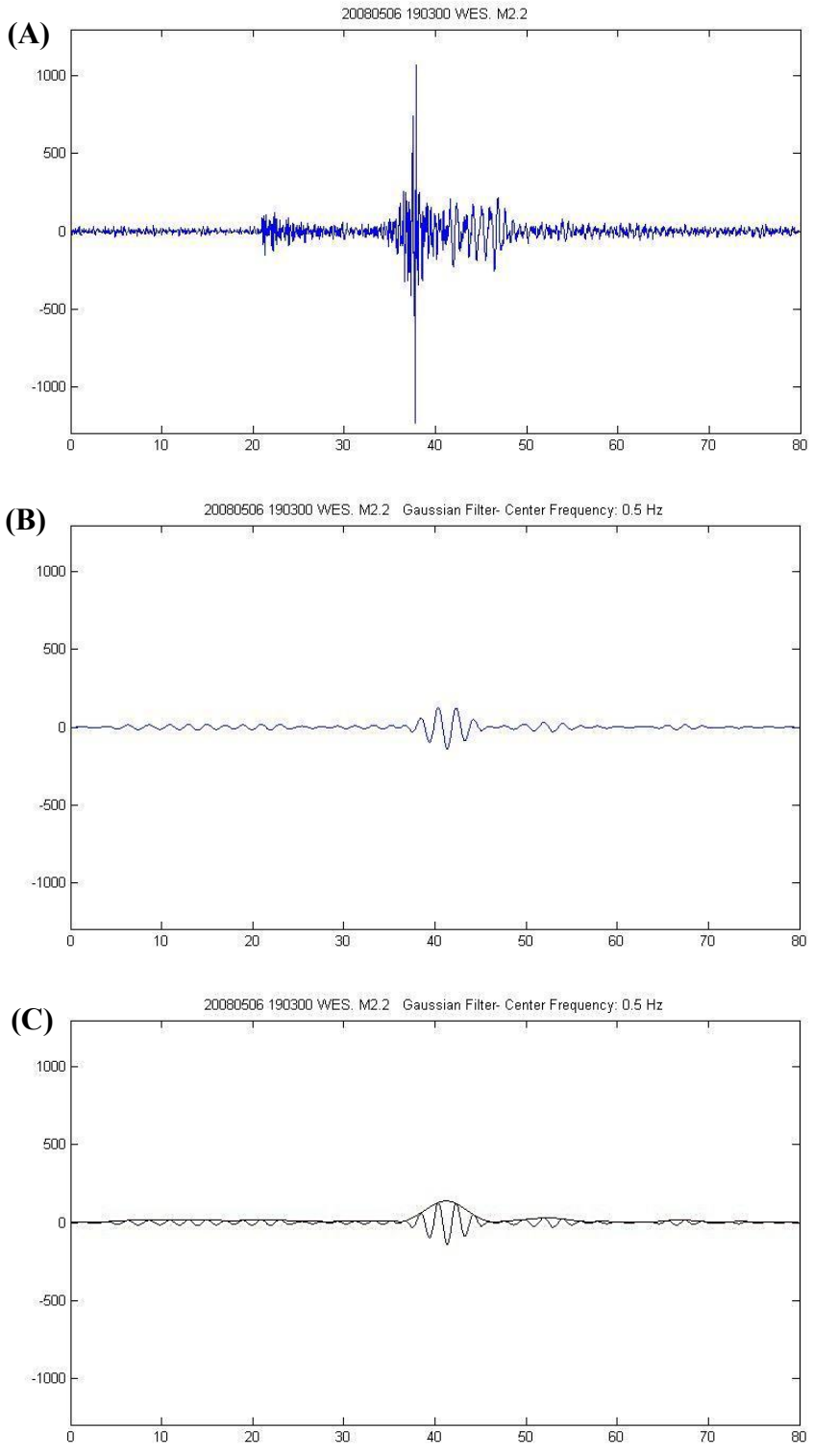
(A)
20080506 190300 WES. M2.2
1000
500
0
-500
-1000
0
10
20
30
40
50
60
70
80
(B)
20080506 190300 WES. M2.2 Gaussian Filter- Center Frequency: 0.5 Hz
1000
500
0
-500
-1000
0
10
20
30
40
50
60
70
80
(C)
20080506 190300 WES. M2.2 Gaussian Filter- Center Frequency: 0.5 Hz
1000
500
0
-500
-1000
0
10
20
30
40
50
60
70
80

(D)

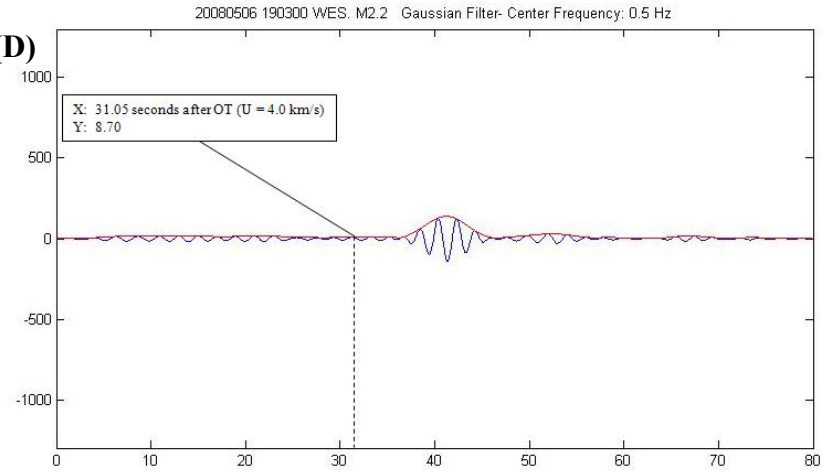

(E)

Group Velocity (km/s)

4.0	22.58	9.92	5.69	9.07	15.61	8.03	7.23	9.46	6.99	3.86	2.03	2.58	3.65	4.43	4.45	4.04	4.62	6.30	7.96	8.70
3.9	5.09	10.65	15.46	6.53	5.21	10.42	8.61	5.82	3.77	2.40	0.89	2.00	3.17	3.55	2.85	0.91	1.89	4.89	7.62	9.11
3.8	20.39	18.94	5.48	8.75	4.53	5.86	6.01	1.86	0.82	2.14	2.57	2.67	3.34	3.98	3.83	3.37	3.98	6.13	8.80	10.50
3.7	7.73	24.68	6.77	7.07	14.35	10.98	6.33	1.81	1.69	2.88	2.19	1.61	3.68	4.57	4.29	5.03	7.12	9.48	11.58	12.64
3.6	4.91	14.83	32.86	4.64	25.66	15.17	4.96	8.39	7.93	7.11	5.17	5.10	5.93	3.77	1.12	6.83	11.36	13.83	14.40	13.60
3.5	32.67	11.75	19.56	19.69	52.82	37.05	26.63	19.01	16.33	22.18	22.47	20.06	16.99	14.38	14.59	17.49	19.61	18.90	15.17	10.23
3.4	37.20	135.10	122.19	121.84	42.93	64.13	68.02	39.37	47.59	61.15	58.54	51.46	44.55	40.22	37.84	35.81	32.29	26.23	17.15	7.47
3.3	110.69	251.19	317.22	447.52	266.08	176.93	170.36	151.81	124.01	100.90	78.98	67.64	64.70	66.11	65.33	61.22	54.74	46.90	38.39	32.72
3.2	57.81	42.24	27.55	89.08	54.96	55.64	82.56	89.52	76.43	59.59	29.86	16.69	53.24	75.33	82.27	83.22	82.90	81.20	77.71	74.17
3.1	26.72	41.17	35.32	67.31	89.51	26.97	12.94	21.49	13.91	48.33	74.08	73.10	70.83	63.35	59.72	76.69	99.60	114.35	120.23	119.65
3.0	21.60	14.81	22.24	26.58	27.74	78.46	83.34	105.32	135.32	148.56	144.82	128.03	95.69	57.68	51.14	84.67	115.65	133.10	139.70	138.83
2.9	22.86	10.90	25.82	9.53	17.75	52.30	61.44	113.65	137.68	111.06	131.21	169.10	179.39	163.49	143.55	129.62	121.64	116.47	112.03	108.19
2.8	22.97	8.79	17.96	29.33	30.11	52.63	88.03	133.88	172.55	166.87	170.13	181.79	172.86	145.10	113.21	85.33	65.96	55.10	49.65	47.83
2.7	4.25	22.26	19.84	24.54	46.76	34.29	88.28	166.40	221.47	204.61	146.25	107.52	81.12	62.23	43.99	26.36	14.39	10.96	9.83	7.15
2.6	4.29	7.02	12.47	41.90	29.81	31.96	70.24	104.82	103.18	70.73	28.65	7.24	6.79	14.99	16.53	12.40	7.29	6.04	8.11	9.71
2.5	6.13	8.93	9.91	6.22	15.18	30.84	28.64	15.27	9.96	23.35	15.98	9.70	9.89	9.87	8.07	3.73	3.26	9.00	14.38	18.72
2.4	5.24	10.07	6.11	12.48	15.61	19.85	22.70	26.24	22.92	18.40	14.71	8.99	8.86	14.32	17.96	19.78	21.20	23.28	26.21	29.10
2.3	13.30	6.64	12.50	12.76	19.57	38.95	42.10	40.17	33.22	28.61	26.51	23.54	19.61	16.33	13.66	12.35	13.94	17.34	21.00	23.82
2.2	7.35	6.31	8.73	14.95	13.27	23.53	23.96	21.05	15.79	13.09	7.09	5.30	7.71	9.51	9.36	8.11	7.48	7.74	7.80	6.85
2.1	1.55	8.93	4.97	15.25	10.76	12.27	8.90	9.63	15.12	14.59	9.78	8.58	8.70	8.19	6.68	4.67	3.46	3.82	5.22	6.88
2.0	10.76	10.69	9.72	2.62	15.81	22.64	26.62	25.61	20.27	12.82	5.97	8.47	10.55	8.90	5.34	2.56	3.13	4.06	4.47	4.92
	0.1	**0.2**	**0.3**	**0.4**	**0.5**	**0.6**	**0.7**	**0.8**	**0.9**	**1.0**	**1.1**	**1.2**	**1.3**	**1.4**	**1.5**	**1.6**	**1.7**	**1.8**	**1.9**	**2.0**

Period (s)

(F)

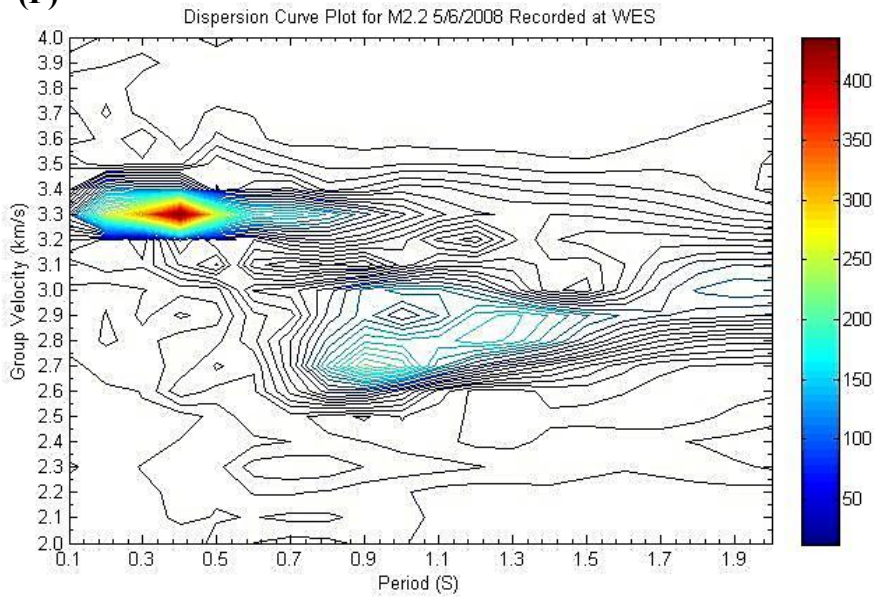

Figure 18 (previous pages): Example of the steps followed in an analysis using the Multiple Filter Technique. An M 2.2 quarry blast from Tilton Sand & Gravel, located in Belmont NH, is used. (A) Seismogram from seismic station WES, located in Weston MA. The source to station distance is 124.2 km. The origin time of the blast is at the 0-second mark, with the P-wave arriving ~20s later. (B) Filtered waveform around a center frequency of 0.5 Hz. (C) The envelope of the filtered waveform, which provides the instantaneous amplitude at any point along the waveform. The instantaneous amplitude is calculated using the Hilbert Transform. (D) Selection of specific values of the envelope determined by the group velocity arrival times. The example shown is the group velocity, U = 4.0 km/s which appears on the WES seismogram at ~31s. For this example, the range of group velocities for which the amplitude value at those times where the group velocities arrive is 2.0 – 4.0 km/s. (E) Matrix of envelope amplitude values for which each amplitude value per group velocity and frequency is entered. Steps B-E is repeated for a range of center frequencies. In this example, the frequency range is between 10 Hz and 0.5 Hz. (F) Dispersion contour plot of the M 2.2 quarry blast WES seismogram. This plot is formed from the completed matrix of (E). Rg is visible between periods 0.7 s to 2.0 s and group velocities of 2.5 to 3.1 km/s. Lg is visible between periods 0.1 s to 0.7 s and group velocities of 3.2 km/s to 3.5 km/s.

The value of α used in this thesis is based on the results of Tu (1990). In order to study the effect of the parameter α on the measurement of Rg group velocity, Tu (1990) tested α values of 5, 20, 50 and 70 on a synthetic seismogram with a known group velocity computed using a crustal structure based on the BADR. Tu (1990) concluded that the value chosen for the parameter α depended upon the nature of the dispersive surface-wave arrivals on the seismogram. The dispersion curve given by $\alpha = 5$ from the synthetic seismogram compared well to observed seismograms with a source-to-station distance of <30 km across the BADR while dispersion curves calculated using $\alpha \geq 20$ compared well to source-to-station distances of >30 km. As discussed in Section 5.6**,** stations within 50 to 170 km are used for this study. Because of this source-to-station range, $\alpha = 20$ is used in this thesis.

5.4 Depth Formula

The goal of the Kafka (1990) method is to provide a quantitative estimate of focal depth for regionally recorded events from observed amplitudes of Rg and Lg waves. The method uses predefined windows of group velocity and period where both Rg and Lg are expected to arrive for events in New England (Table 4). The amplitude values contained in the Rg and Lg windows of Table 4, determined using the MFT, are averaged and these averages are divided by each other to form the Rg/Lg (AVG) ratio at a single station. The Rg/Lg (AVG) ratios for each recording station, for an earthquake at some depth $\boldsymbol{h}$ are averaged together and represented by $\boldsymbol{r(h)}$. The value of $\boldsymbol{r(h)}$ is normalized by $\boldsymbol{r(0)}$ = 1.58 (the $\boldsymbol{r(h)}$ value for an event at the surface, as estimated by Kafka, 1990) and the resulting value is referred to as $\boldsymbol{r_n(h)}$. The value of $\boldsymbol{r_n(h)}$ is used in a semi-empirical formula used to estimate the focal depth of regionally recorded events

$$\boldsymbol{r_n(h) = f(h) + K} \qquad \textbf{(19)}$$

where $\boldsymbol{f(h)}$ is the 0.8s displacement-depth eigenfunction and $\boldsymbol{K}$ is the value of $\boldsymbol{r_n(h)}$ for an event deeper than 5 km. The focal depth of the earthquake is solved for by determining the depth $\boldsymbol{h}$ that satisfies equation (19). The $\boldsymbol{K}$ value is likely to be greater than zero because there is probably some energy, due to background noise, in the various arrival-time vs. period windows even when no Rg is present. Kafka (1990) used a value of $\boldsymbol{K}$ = 0.1 based on the $\boldsymbol{r(h)}$ ratios for two Ardsley, New York earthquakes which had average focal depths of 5.2 km determined from an aftershock survey reported by Locke (1985). I use that same $\boldsymbol{K}$ value for the analysis in this thesis.

5.5 Instrument Correction

The Kafka (1990) method was developed using NESN data from the time period 1990 – 1992. At that time, all NESN stations had similar instrument responses with gains of either ~100 to ~200 counts/micron at 1 Hz (Fig. 19 Top). Due to the similarity of the instrument response between stations, Kafka (1990) did not adjust his method for instrument response. Instead, the instrument response of the NESN stations used in the original development of the Kafka (1990) method is implicit in the constants and application of equation (19). Beginning in 1992, the NESN underwent a series of station upgrades whereby new seismometers and digitizers were installed. By 1994, most NESN stations had new equipment that had a different instrument response from that of the Kafka (1990) data (Fig. 19 Bottom). This change in NESN instrumentation since 1990 means that the Kafka (1990) method cannot be directly applied to waveform data recorded after 1994 unless the difference in instrument responses before and since 1994 is rectified. There are several ways to accomplish this task. For this thesis, I resolve this difference by scaling waveform data recorded with the post-1994 instrument response by a ratio of the pre-1994 to post-1994 instrument responses for frequencies used in this portion of the analysis (0.9 – 10 Hz). Mathematically, this method is described by equation (20).

$$S_{\omega}^{+} = \frac{S_{\omega} \cdot I_{\omega}^{+}}{I_{\omega}} \qquad \textbf{(20)}$$

where S_{ω} is the original post-1994 seismogram in the frequency domain, S_{ω}^{+} is the scaled seismogram in the frequency domain, I_{ω}^{+} is the instrument response of the pre-1994

NESN in the frequency domain and $\boldsymbol{I_\omega}$ is the post-1994 response in the frequency domain.

Next, the inverse Fourier transform is applied

$$\boldsymbol{S_\omega^+ \overset{\mathcal{F}}{\leftrightarrow} S_n} \qquad \textbf{(21)}$$

where $\boldsymbol{S_n}$ is the scaled seismogram in the time domain. Essentially, this method scales the post-1994 waveform to make it appear as though it was recorded on the pre-1994 NESN, thus allowing the implementation of the Kafka (1990) method of equation (19) with waveforms recorded after 1994.

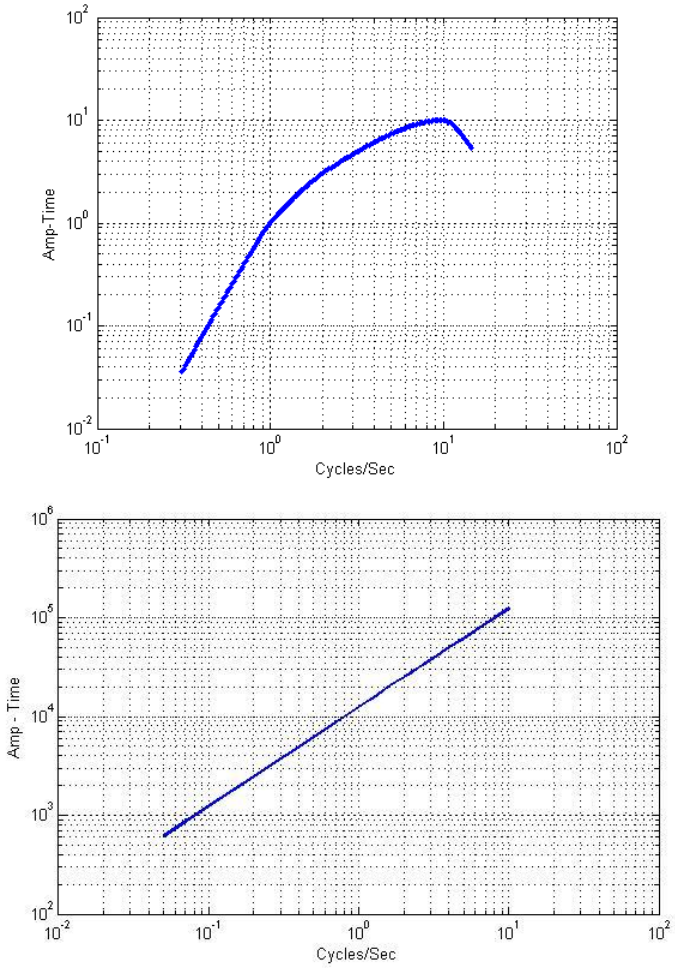

Figure 19: (Top) The measured displacement amplitude response of the New England Seismic Network digital seismograph system up to 1994. (Bottom) The measured displacement amplitude response of the New England Seismic Network from 1994 to the present.

5.6 Rg Limitations

There are several limitations of the Kafka (1990) method. First, the Kafka (1990) method can only use stations with an epicentral range of 50 – 170 km. This is the source-to-station distance range that he used to develop his method based on the data that he had available at that time. Rg/Lg values from stations closer than 50 km did not fit the same trend as Rg/Lg values from stations with an epicentral range of 50 – 170 km, so Kafka (1990) chose not include stations closer to 50 km in his analysis. Also, the Kafka (1990) method estimates earthquake focal depth based on the average of Rg/Lg ratios taken from seismograms from several stations within 50 km to 170 km of the epicenter. The averaging of Rg/Lg ratios compensates for the effects of the source radiation pattern in the amplitudes of the Rg waves recorded at different azimuths around the event. However, some events included in the analysis of this thesis only have Rg/Lg ratios for one or two stations. This affects the accuracy of the estimated focal depth by introducing biases in the estimate of the Rg and Lg amplitudes since instead of sampling the full radiation pattern, the Rg/Lg ratio reflects the Rg and Lg amplitude at whatever point that station is located along the radiation pattern.

5.7 Influence of Noise

Before the implementation of the Kafka (1990) method, it is necessary to quantify which events are large enough that the analysis will yield reliable results. Since the method relies on sampling the amplitudes of energy in the expected arrival-time windows of Rg and Lg, it does not differentiate between amount of signal or noise within those windows. Therefore, since noise in the Rg and Lg windows may be mistaken for signal, a noisy waveform affects the accuracy of the Rg/Lg measurement by introducing biases in the estimate of the Rg and Lg amplitudes. The SNR was computed for each event waveform by taking the average amplitude of the energy in the Lg windows of Table 4 and dividing that average by an average value for noise, which was determined by repeating the same analysis for Lg but on noise that was recorded prior to the P-wave arrival. A cumulative frequency curve was computed for mean (Rg/Lg) observations that lie below different SNR values to determine the SNR at which noise begins to bias the data (Fig. 20). Only waveforms with no Rg determined from a visual inspection of each waveform were included in the measurements reported in Fig. 20. Mean Rg/Lg ratios for an SNR of >3 range between 0.03 to 0.24. Below a SNR of 3, the range of Rg/Lg ratios expands to 0.1 to 1.25. Since there is no Rg present in these waveforms, the increasing scatter of mean (Rg/Lg) found below an SNR of 3 probably arises from the influence of noise in the sampling windows causing a bias in the mean (Rg/Lg) ratio. Therefore, only earthquake waveforms with an SNR above 3 were included in the Rg focal depth analysis.

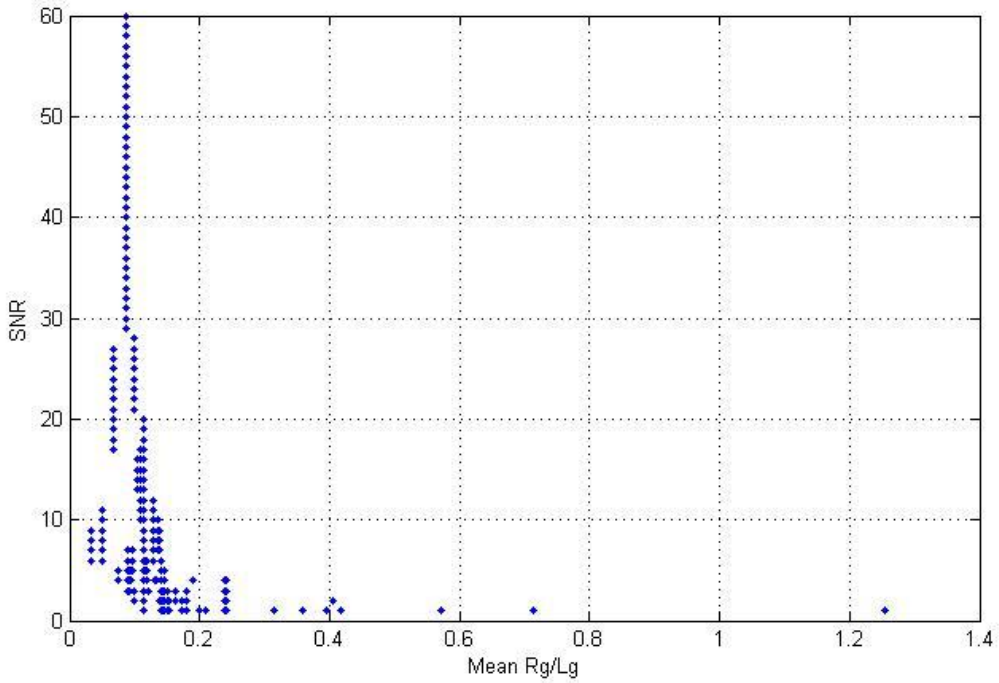

Figure 20: Cumulative frequency curve of mean (Rg/Lg) ratios for different SNR values for earthquake seismograms with no Rg present in the waveforms.

5.8 Focal Depth Estimation Results

Results of the Kafka (1990) method applied to earthquakes in the CNHSZ are found in Table 5. The results indicate that most of the earthquakes occurred deeper than 2-3 km. For several events, there are Rg/Lg values that indicate a focal depth ≥5 km. In these cases, maximum values of the focal depths are estimated based on a series of simulations in HYPO2000. These simulations used synthetic phase data computed for a range of focal depths and used the specific stations and crustal models that were used in the original calculation of the hypocenter of that particular event. The estimate of the maximum focal depth comes from the simulated focal depth. Synthetic phase data associated with a specific simulated focal depth is processed by HYPO2000. HYPO2000 then produces an estimate of the hypocentral information (latitude, longitude, depth and origin time) from that synthetic phase data. The deepest simulated focal depth is considered the maximum value of focal depth for an event, when its synthetic phase data, when processed by HYPO2000, produces a focal depth value that is equal to the original maximum focal depth reported for this event. The original maximum focal depth is the reported focal depth plus the vertical error. The simulated focal depth is the deepest depth for which the earthquake could be located in order for HYPO2000 to produce the focal depth reported in the original earthquake documentation by Weston Observatory.

YYYY/MM/DD	HH:MM:SS.xx	-LAT-	-LON-	-DEP-	Mn	Mc	Average Rg/Lg Ratio, r(h)	$r_n(h)$	Rg Depth
----------	----------	-----	-----	-----	---	---	---------	---------	---------
1990/08/27	06:39:11.38	43.31	71.61	7.93	2.6	2.7	0.12	0.08	5.0 - 9.0
1990/09/17	23:01:37.64	43.4	71.54	7.25	3.1	2.5	0.14	0.09	5.0 - 9.0
1991/07/24	03:33:21.01	43.32	71.54	9.26	2.9	2.8	0.18	0.11	4.6 ± 0.6
1992/03/23	10:01:50.46	43.53	71.64	4.23	3.2	2.7	0.15	0.09	5.0 - 9.4
1992/08/26	23:04:48.94	43.25	71.66	7.58	2.8	2.4	0.10	0.06	5.0 - 6.5
1992/09/09	19:00:51.78	43.34	71.55	6.3	3.2	2.5	0.14	0.09	5.0 - 6.9
1992/10/06	15:38:05.46	43.33	71.56	2.76	3.4	3	0.12	0.07	5.0 - 6.7
1992/10/06	17:05:49.73	43.33	71.54	3.81	2.9	2.4	0.15	0.10	5.0 - 8.6
1996/12/12	19:13:42.65	43.67	71.31	12.32	2.5	2.5	0.23	0.15	3.3 ± 0.6
1998/07/07	09:41:42.44	43.21	71.67	0.17	2.1		0.28	0.18	2.9 ± 0.6
1999/12/10	01:08:51.75	43.24	71.66	8.84	2.1		0.15	0.09	5.0 - 10.6
2000/10/15	23:49:33.03	43.65	71.39	1.05	2.3		0.27	0.17	3.0 ± 0.3
2000/12/16	06:05:09.13	43.73	71.51	10.24	2.4		0.24	0.15	3.26 *
2001/01/03	23:05:29.51	43.65	71.45	20.71	1.6		0.19	0.12	4.07 *
2006/10/26	13:03:03.61	43.5	71.63	7.15	1.8	2	0.09	0.06	5.0 - 8.4
2009/08/19	20:37:29.83	43.27	71.75	1	1.6	2.4	0.16	0.10	5.0 - 6.7
2009/09/09	13:25:06.25	43.65	71.44	13.16	1.9	2.1	0.23	0.15	3.34 *
2009/12/25	20:36:38.27	43.67	71.55	2.57	2.1	2.2	0.24	0.15	3.29 *

Table 5: Rg-based focal depths derived from the Kafka (1990) method of focal depth determination. The asterisk (*) indicates an insufficient number of stations to determine a standard deviation. Rg/Lg ratios per station and the original HYPO depth error per event are found in Appendix C.

The results of the Kafka (1990) method when applied to several earthquakes that occurred in the CNHSZ indicate a range of focal depths from ~3 to 10 km with many events occurring ≥5 km. This is especially true for the events of Cluster A, where each event has an Rg derived focal depth at ≥5 km. When the Rg-derived focal depths are combined with the results of the relative location analysis and the focal mechanisms, it would appear that the source fault of these events, and by implication that of the proposed 1638 earthquake fault, dips eastward with a N-S striking trend, and extends from at least 2-3 km to ≥5 km beneath the Earth's surface.

6.0 Field Survey

In the Central and Eastern U.S. and southeastern Canada, paleoliquefaction studies have contributed more than any other paleoseismic approach to estimating the source areas, magnitudes and recurrence times of large paleoearthquakes (Tuttle and Hartleb, 2012). In brief, these studies usually involve identifying Late Quaternary deposits that are susceptible to liquefaction, searching exposures in these deposits for earthquake-induced liquefaction features, dating the liquefaction features to establish their time of formation, and analyzing the size and distribution of features and the liquefaction potential of their source beds in order to constrain the source area and magnitude of the causative earthquake(s). Several notable liquefaction studies have been conducted in New England and adjacent Quebec indicating that such an approach may be useful in the CNHSZ. They include studies in the meizoseismal areas of the 1727 MLg ~5.5 Newburyport, MA earthquake (Tuttle and Seeber, 1991; Gelinas et al., 1998), the 1925 M_w 6.2 Charlevoix, Quebec earthquake (Tuttle and Atkinson, 2010), and the 1988 M_w 5.9 Saguenay, Quebec, earthquake (Tuttle et al., 1990; Tuttle, 1994). There is currently no direct, physical geologic evidence to tie the 1638 earthquake to the CNHSZ. If any direct evidence does exist, it could be found in the surficial geology of the source region of the earthquake.

The surficial geologic setting most conducive to the formation and recognition of earthquake-induced liquefaction features includes a water-saturated loose, sandy layer overlain by a cohesive non-liquefiable sediment layer (Tuttle and Hartleb, 2012). The cohesive layer promotes the build-up of pore-water pressure in the underlying sandy layer. As seismic waves generated by an earthquake propagate towards the ground

surface, cyclic shear waves in particular distort the structure of near-surface sediments through which they pass. Densely packed soils will tend to dilate and not experience cyclic mobility. However, relatively cohesionless sediment that is water-saturated and loosely packed will tend to compact, leading to an increase in pore-water pressure (Tuttle, 2001). If pore-water pressure increases to the point that it equals overburden pressure, the sediment liquefies and behaves as a viscous liquid. The resulting slurry of water and sediment intrudes the non-liquefiable layer, forming dikes and sills and erupting on the ground surface, forming sand blows or sand boils (Fig. 21; Gelinas et al., 1998). Sand blows burying paleosurfaces, related sand dikes and sills, as well as soft-sediment deformation in the source beds, are the telltale signatures of a paleoearthquake (Tuttle and Hartleb, 2012). Although small earthquakes are known to have induced liquefaction (e.g. 2010 M 4.9 Randolph, Utah Earthquake), these sand injection features generally require a magnitude 5.0 or greater earthquake to generate them and usually originate from a few meters to 15 m depth beneath the surface (Yeats et al., 1997).

Preceding this thesis, a reconnaissance-level search for paleoliquefaction features in New Hampshire was conducted along the Baker River northwest of Plymouth, the Pemigewasset River near Plymouth, and the Merrimack River near Concord (Tuttle et al., 2000). A few soft-sediment deformation structures but no sand dikes and sand blows were found in exposures of Holocene fluvial deposits and Late Pleistocene glaciofluvial and glaciolacustrine deposits. In the areas searched, the sedimentary conditions were not ideal for the formation of earthquake-induced liquefaction features and the recommendation was made that additional reconnaissance be performed along the Pemigewasset River south of Plymouth. For this reason, I conducted a survey along

portions of the Pemigewasset and Merrimack Rivers beginning 5 km south of Plymouth, NH to Boscawen, NH (Fig. 22). In addition, I also surveyed a section of the Winnipesaukee River at the confluence of the Winnipesaukee and Pemigewasset Rivers and the Suncook River avulsion site (Perignon, 2008; Wittkop et al., 2007; Fig. 22, 23).

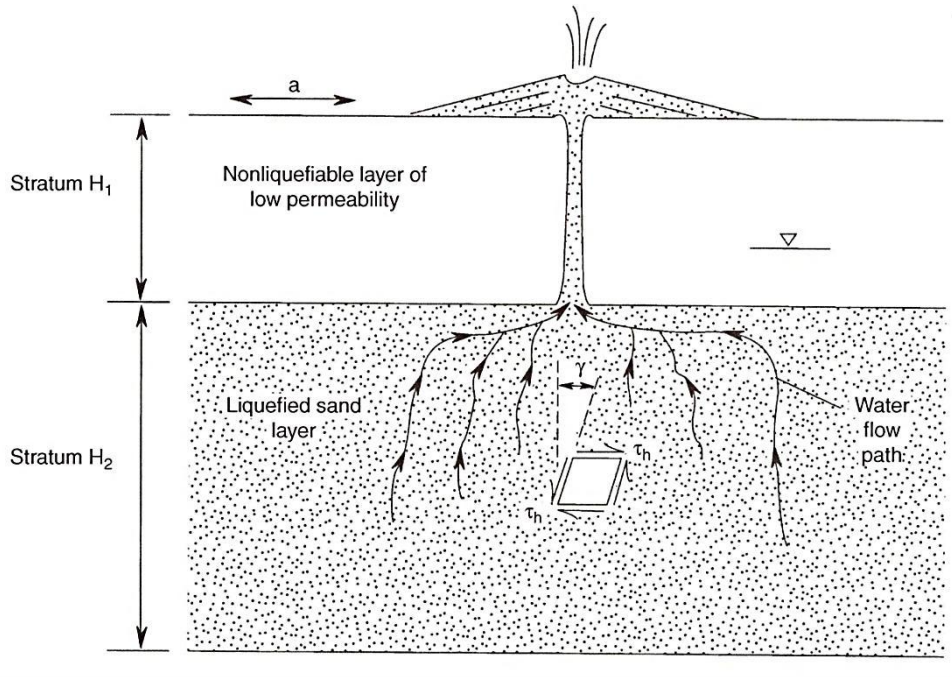

Figure 21: General diagram of the formation of a sand dike and sand volcano or "sand blow". It is a vertical section showing the interaction of sedimentary layers, seismic loading conditions and water flow paths involved in the formation of a sand injection. γ: shear strain (angle in radians), a: horizontal acceleration, τ_h: shear stress induced by horizontal acceleration. Figure from Obermeier (2009).

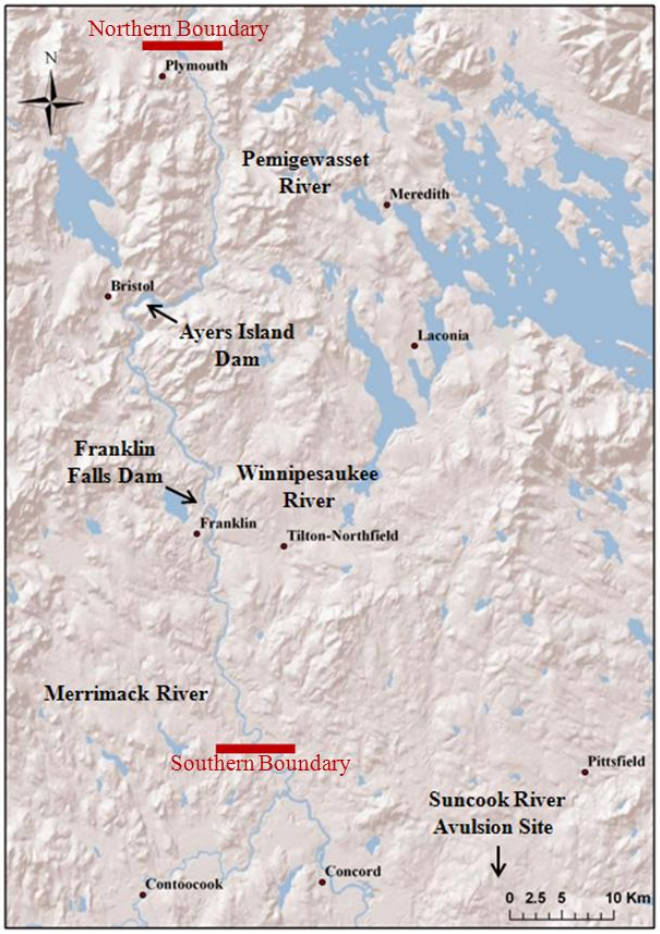

Figure 22: Map of the river survey region. The top red bar indicates the northern extent of the river survey along the Pemigewasset River. The bottom red bar indicates the southern extent of the river survey along the Merrimack River. The Merrimack River forms at the confluence of the Pemigewasset and Winnipesaukee Rivers ~3 km south of Franklin Falls Dam.

Figure 23: (Top) Google Earth© image of the Suncook River Avulsion Site in Epsom NH. The sandy section labeled "Cutter's Pit" is the remains of a small sand and gravel quarry.

6.1 Field Survey Observations

Sediment type and degree of exposure varied along the rivers in the survey area were**.** There were exposures of sandy sediments that lacked an overlying cohesive layer that would promote buildup of pore-pressure and the formation of sand injection features (Fig. 24). Some sections of the Pemigewasset River did not offer any exposures due to the ponding of water of both Ayers Island Dam in Bristol NH and Franklin Falls Dam in Franklin NH. Locally, the dams raised the river level and formed new shorelines set back from the original channel. Extensive vegetation covers the shorelines in those areas**.**

Figure 24: (Left) a ~0.5 m exposure of pebbly coarse sand located ~8.5 km upstream from Ayers Island Dam. (Right) deltaic sediment located at the Merrimack River boat ramp near Boscawen NH. Neither exposure had a clay-rich capping layer that would promote the buildup of pore-water pressure during earthquake shaking.

Several sections of the Pemigewasset and Merrimack Rivers did provide cutbank exposures of sedimentary conditions conducive to the formation of earthquake-induced liquefaction as outlined in the beginning of section 6. In the northern part of the study area, a section of the Pemigewasset River, beginning in Plymouth NH and extending ~4-5 km downstream (Fig. 25 Bottom), provided exposures of silty to sandy rhythmites overlain by coarse-grained sands (Fig. 25 Top). The rhythmites were interpreted as a Late Wisconsin glaciolacustrine deposit while the overlying sandy layer was interpreted as Middle to Late Holocene fluvial deposits (Tuttle et al., 2000). A previous survey conducted in the area by Tuttle et al. (2000) postulated that the silty glaciolacustrine deposits could act as an aquitard for any sandy deposits that might occur below. However, no obvious sand injection features were observed in cutbank exposures along this stretch of river.

In the southern portion of the study area, a stretch of Merrimack, 5 km upstream of Boscawen NH, provided exposure of sedimentary conditions suitable to the formation of liquefaction features (Fig. 26 Bottom). Here, a sediment exposure several meters in length and approximately 0.5 m in height was investigated (Fig. 26 Top). The bottom portion is pebbly coarse sand with some cobbles overlain by fine sands followed by a silty clay layer. Several small diapirs extend from the fine sand layer in to the base of the clay layer. Small sand intrusions can form as the result of earthquake-induced liquefaction and may be indicative of ground shaking near the threshold of liquefaction (Sims, 1973; Tuttle and Atkinson, 2010). Similar dewatering structures due to depositional processes are common in sandy and silty fluvial, lacustrine and deltaic

deposits. Therefore, these types of soft-sediment deformation structures do not necessarily imply genesis by earthquake-induced liquefaction (Gelinas et al., 1998).

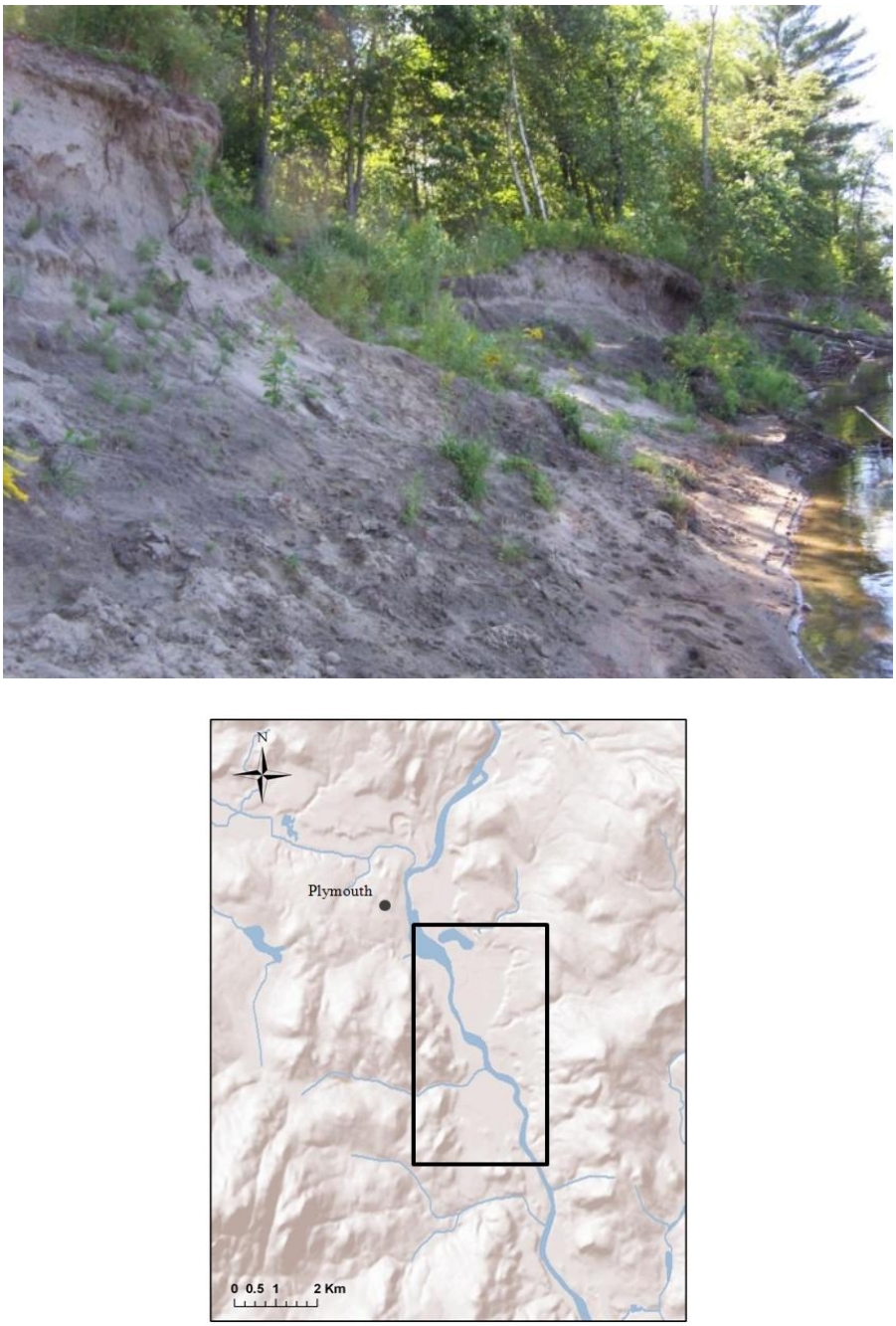

Figure 25: (Top) Example of cutbank exposure commonly found along the outlined section of the Pemigewasset River (Bottom). Exposure is ~3-4 m high and reveals silty and sandy rhythmites overlain by coarse sand.

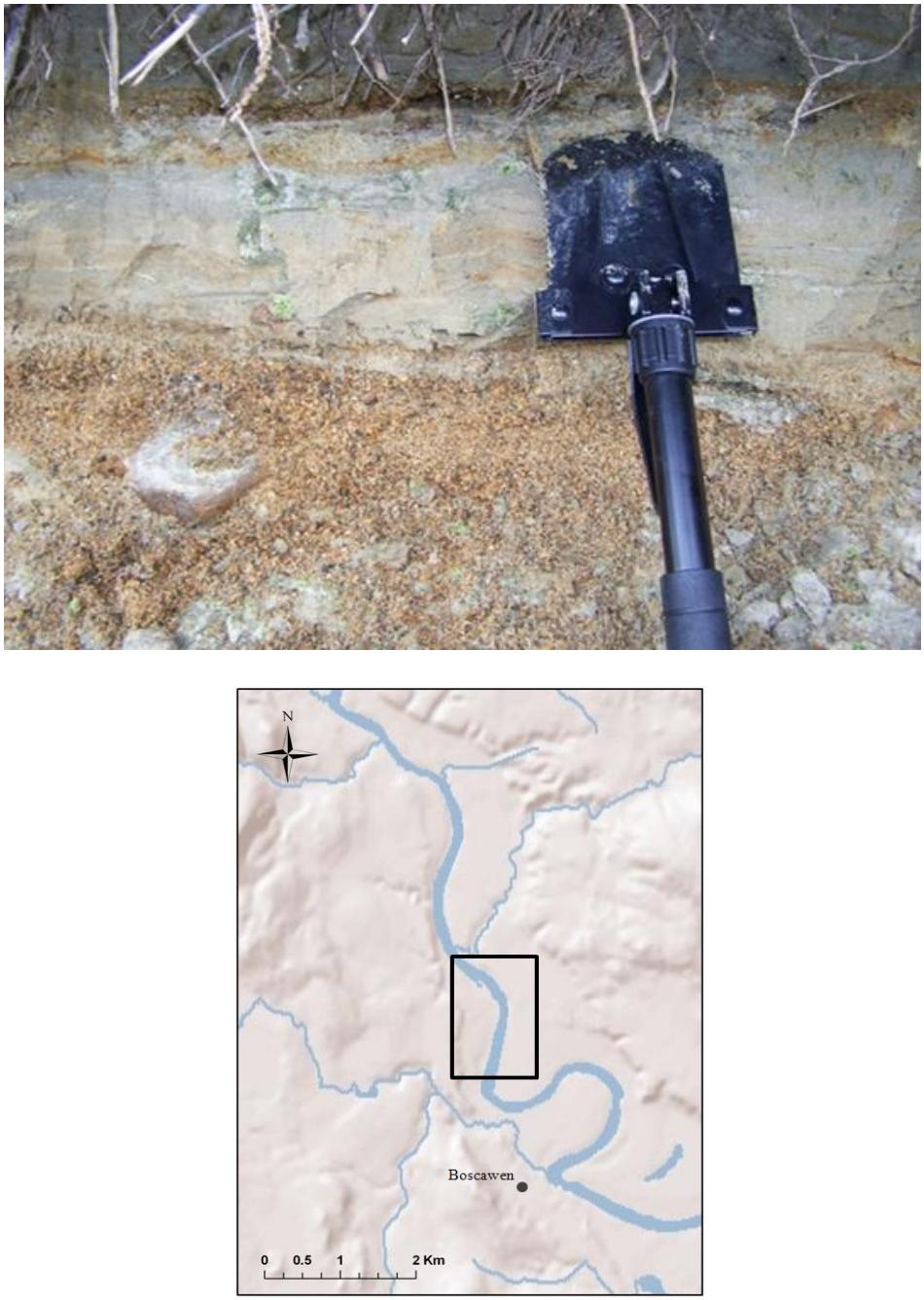

Figure 26: (Left) Outcrop of pebbly coarse sands overlain by fine sands. A silty clay layer overlies the fine sand. Located along the west bank of the outlined section of the Merrimack River (Right). The height of the shovelhead is 12 cm.

During a 100-year flood event on May 15th and 16th 2006, a 2.4 km reach of the Suncook River near Epsom, NH was abandoned in a complete avulsion. 0.8 km of new river channel was incised into wetlands and glacial lake sediment, uncovering large exposures of glacial sand and clays, originally deposited when the avulsion site was once an arm of Glacial Lake Hooksett during the Late Wisconsinan (Perignon, 2008). The sedimentary conditions at the site appear to be conducive to earthquake-induced liquefaction features. Well-sorted, fine to medium-grained sands overlain by a clay layer were found at several locations (Fig. 27). Furthermore, these sands were likely saturated with groundwater since, prior to the avulsion; wetlands existed in portions of the avulsion site next to the now-abandoned river channel (U.S. Geological Survey, 1967). Several small dikes and sills as well as convolute bedding, load coasts, pseudonodules and soft-sediment faults were found and examined throughout the avulsion site by Dr. Martitia Tuttle and myself. The largest dike, 0.5 m in height and 5 cm in width, intrudes a soft-sediment fault below a diamicton (Fig. 28). Convolute bedding is visible primarily within sand layers (Fig. 29), while load casts and pseudonodules (Fig. 30) formed in an interbedded sand, silty and clay unit below the current elevation of a former sand and gravel pit named Cutter's Pit (Fig. 23). In addition to sediment deformation structures, there are numerous soft-sediment faults (Fig. 28).

Figure 27: Favorable sediment conditions for the formation of liquefaction features at the Suncook River Avulsion site. For scale, the notebook is 19.5 cm tall and 11.5 cm wide.

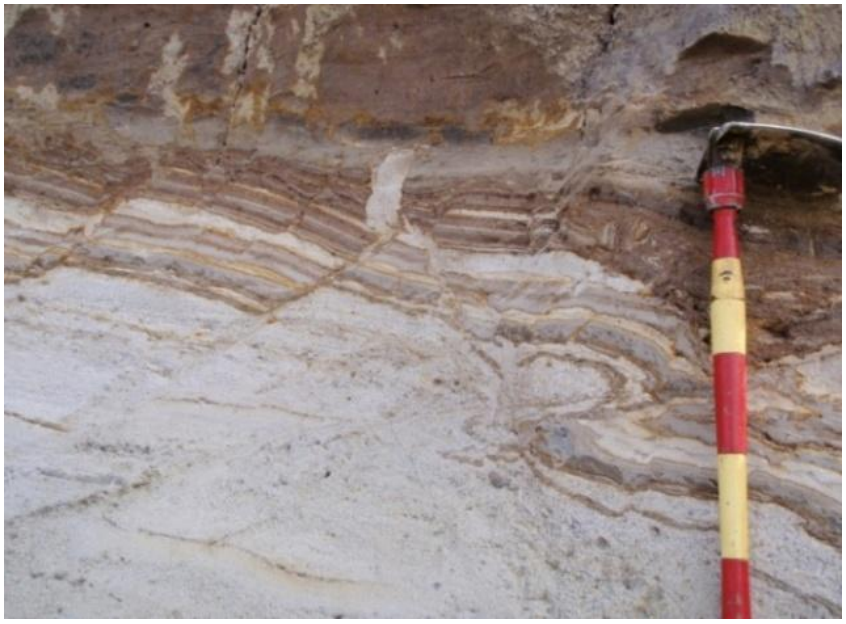

Figure 28: A sand dike located in the Suncook River Avulsion Site. Dikes intrude soft-sediment faults in the interbedded silt and sand deposit immediately below an overlying diamicton. These deformation structures likely formed during the emplacement of the overlying diamicton. For scale, painted intervals on shovel handle represent 10 cm. Photograph by M. Tuttle.

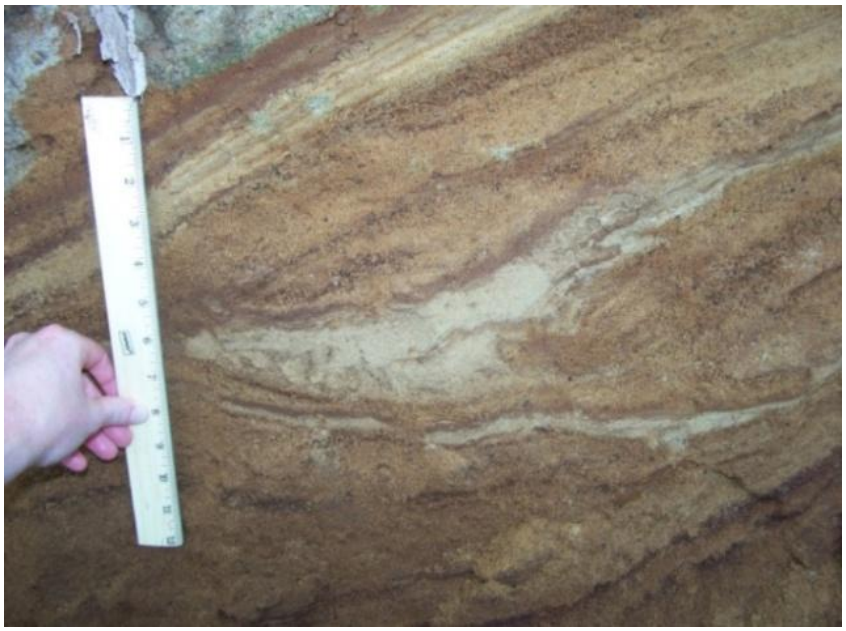

Figure 29: Convolute bedding, which is common throughout the avulsion site. For scale, ruler is 30 cm long.

Figure 30: Load casts and pseudonodules are visible in interbedded sand, silt and clay units. For scale, painted interval on shovel handle represents 10 cm. Photograph by M. Tuttle.

The sand diapirs seen along sections of the Merrimack River, as well as the sand dikes, convolute bedding, load casts and pseudonodules of the Suncook River Avulsion Site, have been previously identified as seismically-induced in other geologic locales (Kundu et al., 2011; Tuttle and Atkinson, 2010; Gelinas et al., 1998; Tuttle and Seeber, 1991; Obermeier et al., 1990; Sims, 1973; Sims, 2012). However, these types of soft-sediment deformation structures are not always indicative of past earthquake activity. Because they are strata-bound and do not disturb the overlying deposits, the deformation structures may be related to depositional processes. Of these features, those that could be related to earthquake-induced liquefaction are the small sand diapirs along the Merrimack River and the convolute bedding, load casts and pseudonodules of the Suncook River Avulsion Site. Pseudonodules occur when the overlying sand layer sinks into the underlying mud layer when that mud layer liquefies. They are known to form due to an external, earthquake-induced shock, which causes the underlying layer to lose strength and the overlying layer to sink into it (Kuenen, 1965). However, they can also form without shaking by a gravity-induced instability where, due to the differential loading of denser, saturated sands overlying less dense, unconsolidated muds, there is a vertical movement of the overlying sands downward into the unconsolidated mud. The formation of pseudonodules due to differential densities of sediment layers is an expression of the Rayleigh-Taylor instability applied to liquidized sands and mud layers (Allen, 1982**).** The sand dikes and soft-sediment faults are folds below the diamicton are likely not related to ground shaking. Since each of the sedimentary features described in this section can have both seismic and non-seismic origins, the presence of these features in the CNHSZ does not necessarily confirm that the region experienced an earthquake of M 5.0 or greater.

7.0 Discussion

In the CNHSZ, the primary geologic structures are the KCMS and the CNHA (Fig. 31). The KCMS is located in the western portion of the survey region and is composed of a series of west verging nappes. Each nappe is bounded by a nappe-propagating thrust that dips east and is rooted in the CNHA. The CNHA is located in the eastern portion of the CNHSZ and acts as a "dorsal zone" which divides the west-verging nappes of the KCMS and the east verging nappes of the LAS. A basal décollement is inferred to lie between these structures and the underlying basement (Brown and Solar, 1999). The thickness of the CMT metasedimentary rocks above the décollement has been estimated to be as thin as 3 km by Eusden and Lyons (1993), but other estimates of the thickness of the metasedimentary rocks range up to 10 km (Thompson et al., 1993; Stewart et al., 1993). The true depth of the décollement between the CMT and the underlying Silurian basement is pertinent to this thesis since it may give insight into the style of active faulting in the CNHSZ. If the actual depth of the décollement is closer to the Eusden and Lyons (1993) estimate of 3 km, this could indicate that a basement-involved thrust is the source of the earthquakes of Cluster A as the Rg-derived focal depths suggest. Those earthquakes that have focal depths shallower than 3 km may occur as the overlying metasediment adjusts to the movement of the underlying basement thrust. If the actual depth of the décollement is closer to 10 km, then perhaps the source fault of the Cluster A earthquakes is along one of the east-dipping thrust faults that form the boundary between the nappes of the KCMS and is rooted in the CNHA. However, since the results of the Rg-derived focal depths only provide a range of focal depths of ~5 to ~10 km, the true focal depths may still lie beneath the décollement in a basement-

involved thrust even if the true depth of the décollement is deeper than the Eusden and Lyons (1993) estimate of 3 km. Further research is necessary to determine the precise depth of the basal décollement, thus providing insight into whether the source fault of Cluster A, and possibly the MLg 6.5 ± 0.5 earthquake of 1638, is a basement-involved thrust or if it took place along one of the now reactivated east-dipping nappe-propagating thrust faults that form the boundary between the nappes of the KCMS (Fig. 31).

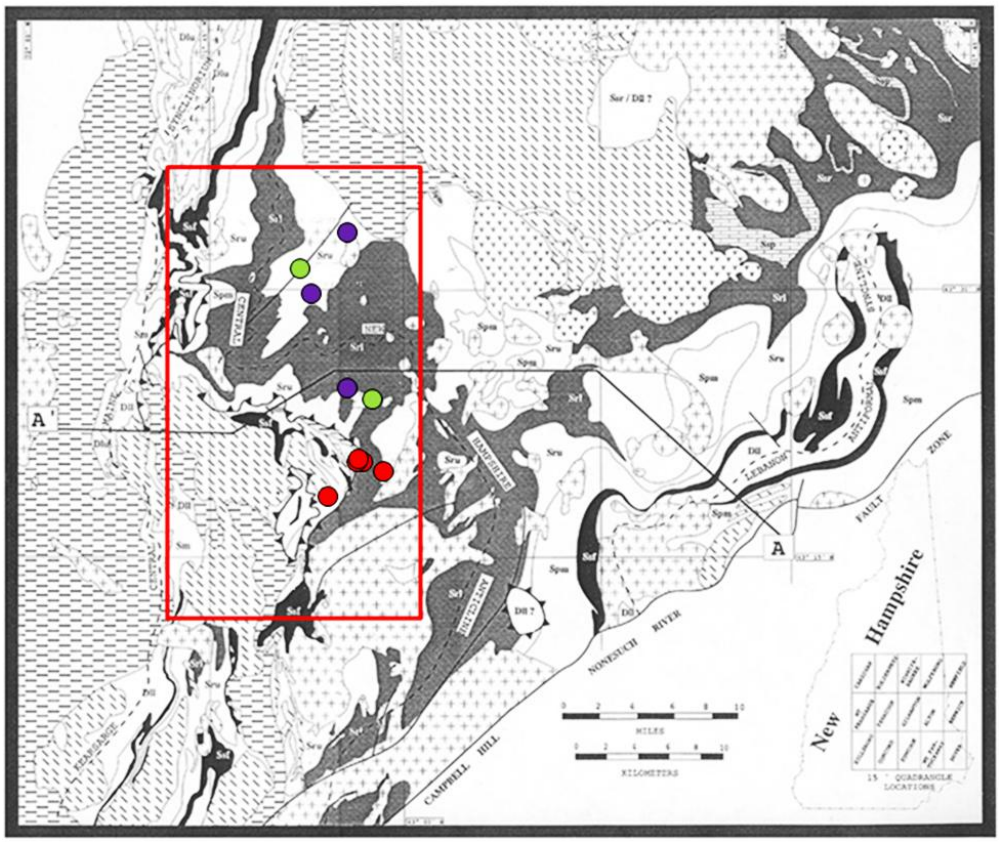

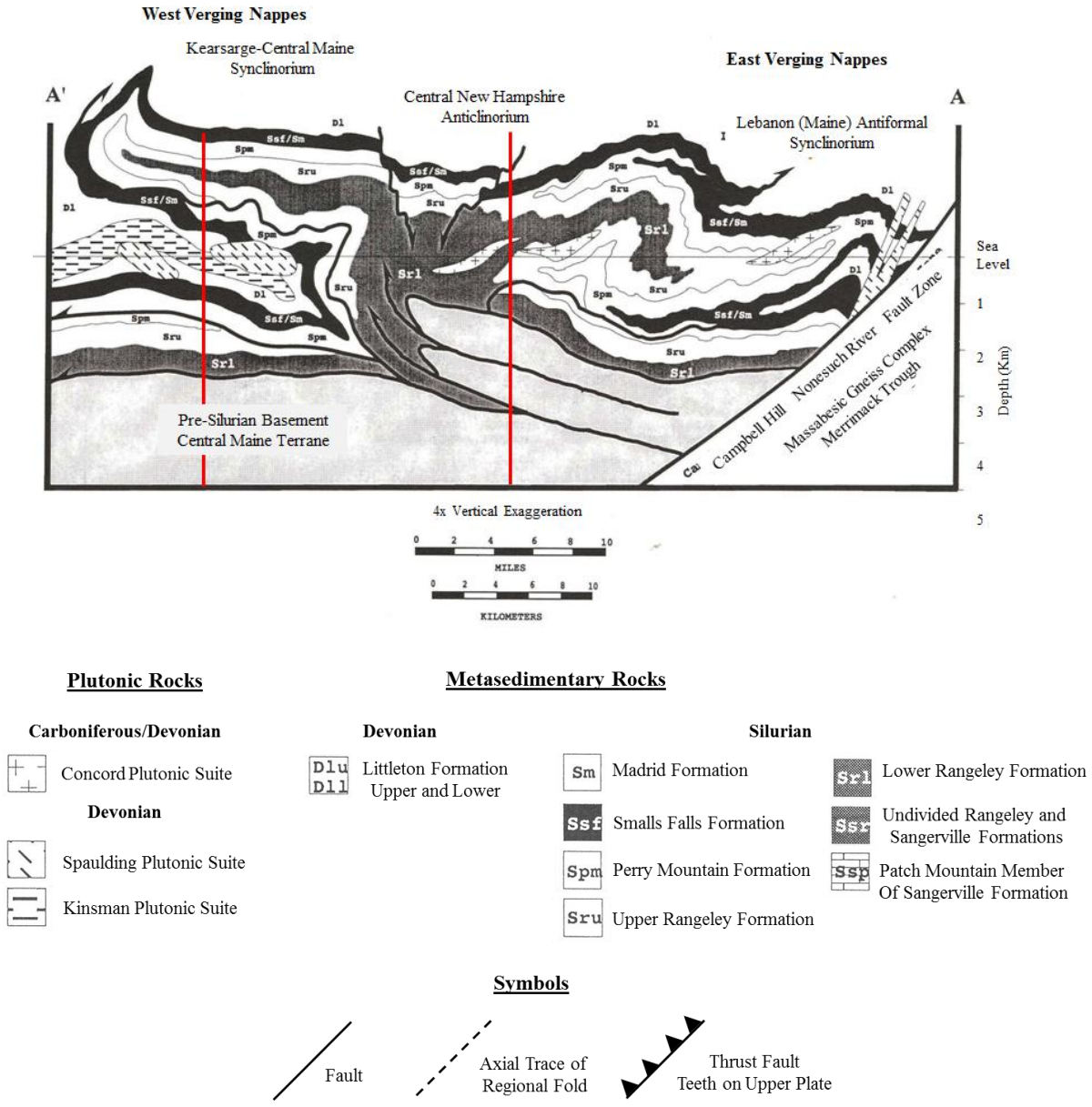

Figure 31: Modified from Fig. 1. Geologic map and cross section through central-eastern New Hampshire from Eusden and Lyons (1993). The A' – A line transects through central New Hampshire. The red rectangle shows the approximate bounds of the study area of this thesis. The colored dots in the map view correspond to earthquake epicenters shown in Fig. 31. The thin line indicating sea level is the approximate erosional level exposed today in central New Hampshire. Eusden and Lyons (1993) place the depth of pre-Silurian basement at 3 km but acknowledge that this depth is poorly constrained. Other estimates place the depth of the top of the pre-Silurian basement up as deep as 10 km (Thompson et al., 1993; Stewart et al., 1993).

In the northeast United States, it is not clear whether faults mapped at the Earth's surface are the same faults that are generating earthquakes (Ebel and Kafka, 1991). Any connection between current seismicity and mapped geologic structures would be beneficial to the understanding of active faulting in New England. Therefore, a pertinent question is whether the possible source fault of the MLg 6.5 ± 0.5 earthquake of 1638, as well as of the modern earthquakes, has any surficial expression. Using the relocated hypocenters of Cluster A, the minimum focal depth of Cluster A from the Kafka (1990) method, and the strikes and dips of the nodal planes from the focal mechanisms of Section 4 as well from the 1982 Gaza and 1986 Northfield earthquakes, a possible surface location of the fault would lie ~7 km west of the Mn 3.2 09/09/1992 master event epicenter (Fig. 32). Since the results of the Kafka (1990) method only give a minimum focal depth, the surface expression may lie farther to the west depending on the focal depths of the events. The projected surface expression of the fault may also shift ±4 km E-W due to error in the absolute epicentral determination of the master event.

The obvious geomorphological features in this region are the Pemigewasset and Merrimack rivers that appear to flow NNW – SSE roughly parallel to the extrapolated surface expression of a postulated seismogenic fault that may be the source of modern seismicity and the 1638 earthquake. Tectonic loading from thrusts can cause a gentle warping of the crustal interior, which can result in the tilting of contemporary topographic structures. Rivers are particularly sensitive to such tilting because of the gradient changes imposed by that tilting (Holbrook and Schumm, 1999; Burnett and Schumm, 1983). It is speculation, but if the fault structure of the CNHSZ has affected the topography of the region, then it is possible that the courses of the Pemigewasset and

Merrimack rivers are somewhat influenced by this tilting and that sedimentary deposits from these rivers may be covering the fault trace. A similar situation exists in the Ventura Basin in California where the Santa Clara River flows along portions of the fault trace of the Oak Ridge Fault, north of South Mountain-Oak Ridge. Holocene deposits from the Santa Clara River actively cover the surface expression of the Oak Ridge Fault trace (Yeats, 1988).

The surficial geology of the CNHSZ is generally mixed in terms of potential for forming seismically induced liquefaction features. Many cutbank exposures reveal thick layers of sands with no overlying clay layer that would promote the buildup of pore-water pressure and liquefaction in the sand layers in response to strong round shaking. However, some sedimentary sections, such as those in the Suncook River Avulsion Site and along the Merrimack River near Boscawen, have a higher potential to have experienced liquefaction as they include interbedded sand, silt and clay that are more conducive to the formation of liquefaction features. In these locations, sand dikes, convolute bedding, load casts and pseudonodules were found. These soft-sediment deformation structures can have both seismic and non-seismic origins. Other paleoliquefaction surveys in New England have reached similar conclusions. Prior surveys along the Baker River and sections of the Pemigewasset and Merrimack Rivers by Tuttle et al. (2000) and of the Ossipee Lakes region by Gelinas et al. (1998) both found soft-sediment deformation structures similar to those found during this study in the Suncook River Avulsion Site and along the Merrimack River. Both surveys concluded that, although seismic origin could not be ruled out, they were likely penecontemporaneous and not related to Holocene seismicity. The findings of this survey

are inconclusive. The small sand dikes along the Merrimack River and the convolute bedding, load coasts and, pseudonodules of the Suncook River Avulsion site are tantalizing, but they cannot be used as direct evidence to support the hypothesis that the MLg 6.5 ± 0.5 earthquake of 1638 was centered in the CNHSZ.

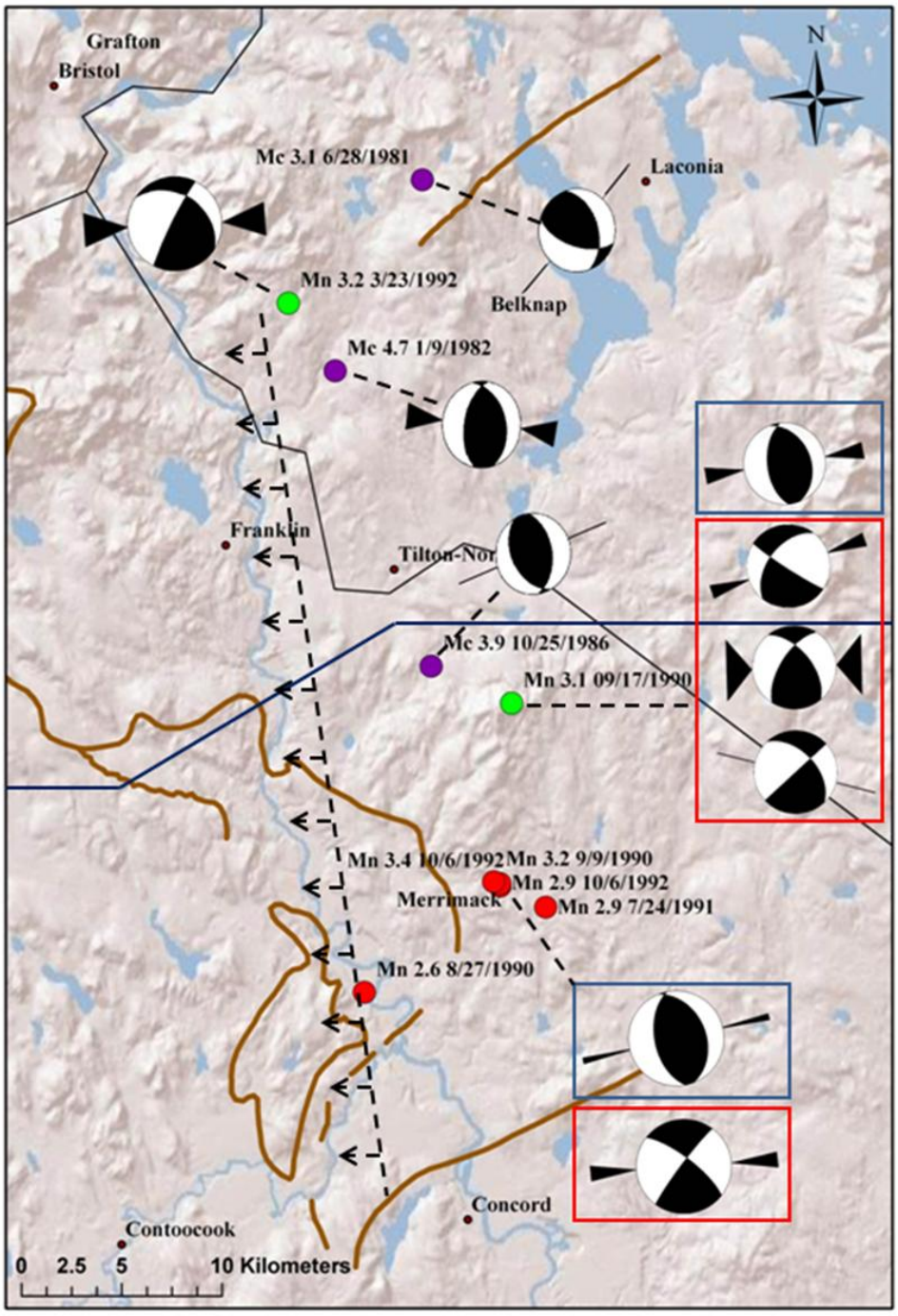

Figure 32 (Previous Page): Projected fault expression (Dashed Line with Arrows) based on the minimum focal depth of 5 km for the Mn 3.2 9/9/1992 relative location master event, derived using the Kafka (1990) method, the dip direction from the relative location analysis and the strike and dip angles from the focal mechanisms section. The surface expression may extend farther to the west as focal depth increases (Arrows). The line length is ~47 km and is based on the proposed "aftershock length" of the MLg 6.5 ± 0.5 earthquake of 1638 from Ebel et al. (2000). (Red Dots) Relocated absolute hypocenters of Cluster A. (Green Dots) The Mn 3.1 9/17/1990 and Mn 3.2 3/23/1992 earthquakes. (Purple Dots) The Gaza (Mc 4.7 1/19/1982), Northfield (Mc 3.9 10/25/1986) and Laconia (Mc 3.1 6/28/1981) earthquakes. (Brown Lines) Mapped faults in the region. (Blue Line) The A'-A transect through the study area. (Blue Square) Focal mechanism solutions with station WNH as a reversed polarity, dilatational first arrival. (Red Square) Focal mechanism solutions with station WNH as a corrected-polarity, compressional first arrival.

8.0 Conclusion

Three geophysical techniques were used to analyze recent, digitally recorded seismic data for earthquakes that have occurred within the past few decades within the CNHSZ to understand the geometric orientation of a hypothesized source fault of the MLg 6.5 ± 0.5 earthquake of 1638. The first geophysical technique is a master-event relative location analysis. Results of the relative locations indicated a possible eastward dip of the source fault. Focal mechanisms computed for several events within the CNHSZ, as well as previous fault plane solutions from the region, when combined with the results of the relative location analysis, suggest that this eastward dipping structure has a NNW-SSE trend. Rg-derived focal depths place the Cluster A of the relative location analysis at a minimum focal depth of 5 km. Based on the absolute focal depths, the source fault may be a basement-involved thrust fault or one of the east-dipping thrust faults that form the boundary between the nappes of the KCMS. Further research is necessary to determine the depth of the pre-Silurian basement in the region, which would clarify the type of fault in the CNHSZ. In either case, when extrapolated updip to the surface, the fault roughly corresponds with the Pemigewasset-Merrimack River Valley. It is speculated in this thesis that topographic tilting from crustal deformation due to the source fault may influence the courses of both rivers. In addition, a field survey of portions of the Pemigewasset, Merrimack and Winnipesaukee Rivers as well as the Suncook River Avulsion site, was undertaken to search for seismically-induced liquefaction structures. This survey resulted in the discovery of several small-scale liquefaction features. Although some of the features may be the result of ground shaking, all of these features are strata-bound and therefore may be non-seismic in origin. The

results of the survey are inconclusive in supporting the hypothesis that the MLg 6.5 ± 0.5 earthquake of 1638 was centered in the CNHSZ.

9.0 Works Cited

Allen, J. R. L., 1982, Developments in Sedimentology, Sedimentary Structures: Their Character and Physical Basis, Volume II, Elsevier, Amsterdam-Oxford-New York.

Bennett, D. S, , Wittkop, C. A., and Dicken, C. L., 2006 , Bedrock Geologic Map of New Hampshire - A Digital Representation of the Lyons and others 1997 map and ancillary files: U.S. Geological Survey Data Series 215, scale 1:250,000, CD-ROM.

Bradford, W. 1952 edition, *Of Plymouth Plantation 1620-1647*, S.E. Morison, ed., Alfred A. Knopf, New York, p. 448.

Bouchon, M., 1982, The Complete Synthesis of Seismic Crustal Phases at Regional Distances, Journal of Geophysical Research, v. 87, p. 1735–1741.

Brown, M., Solar, G. S., 1999, The mechanism of ascent and emplacement of granite magma during transpression: a syntectonic granite paradigm, Tectonophysics, v. 312, p. 1–33.

Burnett, A. W., Schumm, S. A., 1983, Alluvial river response to neotectonic deformation in Louisiana and Mississippi, Science, v. 222, p. 49-50.

Campillo, M., Bouchon, M., Massinon, B., 1984, Theoretical Study of the Excitation, Spectral Characteristics and Geometrical Attenuation of Regional Seismic Phases, Bulletin of the Seismological Society of America, v. 74, p. 79–90.

Campillo, M., 1990, Propegation and Attenuation Characteristics of the Crustal Phase Lg, Pure and Applied Geophysics, v. 132, no. 1-2, p. 1–19.

Doll, C., 1992, A study of New England seismicity with emphasis on Massachusetts and New Hampshire, Quarterly Progress Report and Earthquake Bulletin, Earth Resources Laboratory, MIT, Cambridge, Massachusetts.

Dziewonski, A. M., Bloch, S., Landisman, M., 1969, A technique for the analysis of transient seismic signals, Bulletin of the Seismological Society of America, v. 59, p. 427-444.

Ebel, J. E., Moulis, A. M., Smith, D., Hagerty, M., 2008, The 2006-2007 Earthquake Sequence at Bar Harbor, Maine, Seismological Research Letters, v. 79, no. 3, p. 457–478.

Ebel, J. E., 1996, The Seventeenth Century Seismicity of Northeastern North America. Seismological Research Letters, v. 67, no.3, p. 51–68.

Ebel, J. E., Bonjer. K. P., Oncescu, M.C., 2000, Paleoseismicity: Seismicity evidence for past large earthquakes. Seismological Research Letters, v. 71, no. 2, p. 283–294.

Ebel, J. E., Bouck, B. R., 1988, New Focal Mechanisms for the New England Region: Constraints on the Regional Stress Regime, Seismological Research Letters, v. 59, no.4, p. 183–187.

Ebel, J. E., 1985, A Study of Seismicity and Tectonics in New England, Final Report, Division of Radiation Programs and Earth Sciences, Office of Nuclear Regulatory Research, U.S Nuclear Regulatory Commission.

Ebel, J. E., 2010, A Study of New England Seismicity, Quarterly Earthquake Report October–December 2009: Weston Observatory, Department of Geology and Geophysics, Boston College.

Ebel, J. E., 1992, A Study of New England Seismicity, Quarterly Earthquake Report January–March 1992: Weston Observatory, Department of Geology and Geophysics, Boston College.

Ebel, J. E., Kafka, A. L., 1991, Earthquake activity in the Northeastern United States, The Geology of North America, Decade Map Volume I, p. 277-290.

Ellsworth, W. L., Roecker, S. W., 1981, Sensitivity of the earthquake location problem to network geometry, in Seismicity and Tectonics of the Pamir-Hindu Kush Region of Central Asia [Ph.D. Thesis]: Cambridge, Massachusetts Institute of Technology, 296 p.

Eusden, J. D., Jr., Lyons, J. B., 1993, The sequence of Acadian deformations in central New Hampshire, *in* Roy, D. C., and Skehan, J. W., eds., The Acadian Orogeny: Recent Studies in New England, Maritime Canada, and the Autochthonous Foreland: Boulder, Colorado, Geological Society of America Special Paper 275.

Franzi, D., Wittkop, C., Koteff, C., 2008, Surficial Geologic Map of the Concord Quadrangle, Merrimack County, New Hampshire, U.S. Geological Suvey, 1:24,000.

Gelinas, R., Cato, K., Amick, D., Kemppinen, H., 1998, Paleoseismic Studies in the Southeastern United States and New England: U.S. Nuclear Regulatory Commision, NUREG/CR 6274.

Gephart, J. W., Forsyth, D. D., 1985, On the state of stress in New England as determined from earthquake focal mechanisms, Geology, v. 13, p. 70-72.

Gomberg, J. S., Shedlock, K. M., Roecker, S. W., 1990, The effect of S-wave arrival times on the accuracy of hypocenter estimation, Bulletin of the Seismological Society of America, v. 80, p. 1605 – 1628.

Herrmann, R. B., Ammon, C. J., 2002, Computer Programs in Seismology: Surface Waves, Receiver Functions and Crustal Structure, Version 3.30, St. Louis University.

Hughes, S., Luetgert, J. H., 1991, Crustal Structure of the Western New England Appalachians and the Adirondack Mountains, Journal of Geophysical Research, v. 96, no. B10, p. 16,471–16,494.

Jesuit Relations, The Jesuit Relations and Allied Documents- Travels and Explorations of the Jesuit Missionaries in New France 1610-1791,R.G. Thwaites, ed., 14, 261.

Kafka, A. L., 1990, Rg as a depth discriminant for earthquakes and explosions: A case study in New England, Bulletin of the Seismological Society of America, v. 80, no.2, p. 373-394.

Kafka, A. L., 1988, Earthquakes, geology and crustal features in southern New England, Seismological Research Letters, v. 59, p. 173–181.

Kafka, A. L., Reiter, E. C., 1987, Dispersion of Rg waves in southeastern Maine: evidence for lateral anisotropy in the shallow crust, Bulletin of the Seismological Society of America, v. 77, p. 925-941.

Kafka, A. L., Dollin M. F., 1985, Constraints on lateral variation in upper crustal structure beneath southern New England from the dispersion of Rg waves, Geophysical Research Letters, v. 12, p. 235–238.

Klimkiewicz, G. C., 1982, Reassessment of ground motion models for the northeast, Earthquake Notes, v. 53, no.3, p. 23-24.

Kuenen, P. H., 1965, Value of experiments in geology, Geologie en Mijnbouw, v. 44, p. 22-36.

Kundu, A., Goswami, B., Eriksson, P. G., Chakraborty, A., 2011, Palaeoseismicity in relation to basin tectonics as revealed from soft-sediment deformation structures of the Lower Triassic Panchet formation, Raniganj basin (Damodar valley), eastern India, Journal of Earth Systems Science, v. 120, no. 1, p. 167-181.

Locke, K., 1985, Quarterly Seismicity Bulletin of the New York-New Jersey Network, 1 October-31 December 1985, Lamont-Doherty Geological Observatory of Columbia University, Palisades, New York.

Ludman, A., Hopeck, J.T., Brock, P. C., 1993, Nature of the Acadian orogeny in eastern Maine, *in* Roy, D. C., and Skehan, J. W., eds., The Acadian Orogeny: Recent Studies in New England, Maritime Canada, and the Autochthonous Foreland: Boulder, Colorado, Geological Society of America Special Paper 275.

Macherides, A., 2003, The Development of a Moment-Magnitude Based Earthquake Catalog for the Northeastern United States [M.S. Thesis]: Chestnut Hill, Boston College, 81 p.

McTigue, J. W., 1986, Modeling Upper Crustal Structure in Southern New England Using Short-Period Rg Waves [M.S. Thesis]: Chestnut Hill, Boston College, 68p.

Obermeier, S. F., 2009, Using Liquefaction-Induced and Other Soft-Sediment Features for Paleoseismic Analysis, *in* McCalpin, J. P., editor, Paleoseismology, Elsevier Inc, Oxford, 504p.

Obermeier, S. F., Jacobson R.B., Smoot, J. P., Weems, R.E., Gohn, G.S., Monroe, J.E., Powars, D.S., 1990, Earthquake-Induced Liquefaction Features in the Coastal Setting of South Carolina and in the Fluvial Setting of the New Madrid Seismic Zone, U.S. Geological Survey Professional Paper 1504.

Pavlis, G. L., 1992, Appraising relative earthquake location errors, Bulletin of the Seismological Society of America, v. p. 82, 836–859.

Perignon, M.C., 2008, Sediment wave-induced channel evolution following the 2006 avulsion of the Suncook River in Epsom, New Hampshire [M.S. Thesis]: Cambridge, Massachusetts Institute of Technology, 95 p.

Press, F., Ewing, M., 1952, Two Slow Surface Waves Across North America, Bulletin of the Seismological Society of America, v. 42, no. 3, p. 219-228.

Pulli, J. J., Toksoz, M. N., 1981, Fault Plane Solutions for Northeastern United States Earthquakes, Bulletin of the Seismological Society of America, v. 71, no. 6, p. 1875-1882.

Ridge, J. C., Canwell, B. A., Kelly., M. A., Kelley, S. Z., 2001, Atmospheric 14C Chronology for Late Wisconsinan Deglaciation and Sea-Level Changes in Eastern New England using Varve and Paleomagnetic Records, Geological Society of America, Special Paper 351, 2001.

Shi, J., Richards, P. G., Kim, W., 2000, Determination of Seismic Energy from Lg Waves, Bulletin of the Seismological Society of America, v. 90, no.2, p. 483-493.

Sims, J. D., 1973, Earthquake-induced structures in sediments of Van Norman Lake, San Fernando California, Science, v. 182, p. 161-163.

Sims, J. D., 2012, Earthquake-induced load casts, pseudonodules, ball-and-pillow, and convolute lamination: Additional deformation structures for paleoseismic studies, *in* Cox, R. T., Tuttle, M. P., Boyd, O. S., and Locat, J., eds., Geological Society of America, Special Paper 493, p. 191-201.

Snoke, J. A., 2009, FOCMEC: Package for determining and displaying earthquake focal mechanisms. http://www.iris.edu/software/downloads/processing/

Stewart, D. B., Wright, B. E., Unger, J. D., Jutchinson, D. R., 1993, Global geoscience transect 8: Quebec- Maine – Gulf of Maine transect, southeastern Canada, northeastern United States of America: United States Geological Survey map I-2329, scale 1:1,000,000.

Thompson, J. B., Bothner, W. A., Robinson, P., Isachsen, Y. M., Klitgord, K. D., 1993, A guide to continental – ocean transect E-1, Adirondacks to Georges Bank, Centennial continent – ocean transect #17: Geological Society of America, 55 p.

Thrane, N., 1984, The Hilbert Transform: Technical Review, No. 3. Brüel&Kjær, BV 0015, 1984.

Tinkham, D. J., Brooks, J. A., 2009, Surficial Geologic Map of the Bristol Quadrangle, Belknap, Grafton and Merrimack Counties, New Hampshire, U.S. Geological Survey, 1:24,000

Tu, Z., 1990, A Study of Rg Wave Dispersion in New Hampshire and Vermont [M.S. Thesis]: Chestnut Hill, Boston College, 96 p.

Tuttle, M. P., 2001, The use of liquefaction features in paleoseismology: Lessons learned in the New Madrid seismic zone, central United States, Journal of Seismology, v. *5*, p. 361-380.

Tuttle, M., Law, T., Seeber, L., and Jacob, K., 1990, Liquefaction and ground failure in Ferland, Quebec, triggered by the 1988 Saguenay Earthquake, Canadian Geotechnical Journal, v. 27, p. 580-589.

Tuttle, M. P., Sims, J.D., Roy, D., 2000, Paleoseismology Investigations in the Greater Boston, Massachusetts Area: Collaborative Research M. Tuttle & Associates, John Sims & Associates, and Boston College. Final Report for U.S. Geological Survey Award No: 1434-HQ-98-GR-00001.

Tuttle, M. P., Seeber, L. 1991, Historic and Prehistoric Earthquake-Induced Liquefaction in Newbury, Massachusetts, Geology, v. 19, p. 594 – 597

Tuttle, M. P., 1994, The liquefaction method for assessing paleoseismicity, U.S. Nuclear Regulatory Commission, NUREG/CR-6258, 38 p.

Tuttle, M. P., and Atkinson, G. M., 2010, Localization of large earthquakes in the Charlevoix seismic zone, Quebec, Canada during the past 10,000 years, Seismological Research Letters, v. 81, n. 1, p. 18-25.

Tuttle, M. P., and Hartleb, R., 2012, Central and eastern U.S. paleoliquefaction database, uncertainties associated with paleoliquefaction data, and guidance for seismic source characterization, Appendix E. *in* Technical Report, Central and Eastern U.S. Seismic Source Characterization for Nuclear Facilities, Technical Report, EPRI, Palo Alto, CA, U.S. DOE, and U.S. NRC, 135 p. plus database.

U.S. Geological Survey, *Gossville Quadrangle*, *New Hampshire,* 1:24,000, 7.5 Minute Series, Washington D.C: USGS, 1967.

Waldhauser, F., Ellsworth, W. L., 2000, A double difference earthquake location algorithm: Method and application to the Northern Hayward Fault, California. Bulletin of the Seismological Society of America, v. 90, no. 6, p. 1353-1368.

Winthrop, J. 1908 edition, *Winthrop's Journal, "History of New* England", 1630-1649, in 2 volumes, reprinted 1959, J.K. Hosmer, ed., Barnes & Noble, Inc., New York, NY. (Vol. 1, P.335; Vol.2, P.373).

Winthrop, J., 1944, Winthrop Papers, Volume IV, 1638-1644, published by the Massachusetts Historical Society, 1944.

Wittkop, C., Dyer, W. P., 2007, Geomorphic Response to Rapid Fluvial Change: the 2006 Suncook River Avulsion, Epsom, New Hampshire, Geological Society of America, 2007 Conference, Oct. 28-31.

Yeats, R. S., Sieh, K., Allen, C. R., 1997, The Geology of Earthquakes. Oxford University Press, New York.

Yeats, R. S., 1988, Oak Ridge Fault, Ventura Basin, California: Slip Rates and Late Quaternary History, Open-File Report 89-343, United States Geological Survey.

Appendix A: Cross-Correlation Values and Time Shifts used in Section 3

Event Date	Event Time	Event Magnitude	Subdirectory Name	Station Name	P Xcorr Value	P Xcorr Diff	P Time Diff (sec)	S Xcorr Value	S Xcorr Diff	S Time Diff (sec)
1992/09/09	19:00:51.78	3.2	22531903	ONH						
1992/09/09	19:00:51.78	3.2	22531903	PNH						
1992/09/09	19:00:51.78	3.2	22531903	DNH						
1992/09/09	19:00:51.78	3.2	22531903	WNH						
1992/09/09	19:00:51.78	3.2	22531903	WFM						
1992/09/09	19:00:51.78	3.2	22531903	GLO			Master Event			
1992/09/09	19:00:51.78	3.2	22531903	WES						
1992/09/09	19:00:51.78	3.2	22531903	IVT						
1992/09/09	19:00:51.78	3.2	22531903	BNH						
1992/09/09	19:00:51.78	3.2	22531903	UXB						
1992/09/09	19:00:51.78	3.2	22531903	MD2						
1992/09/09	19:00:51.78	3.2	22531903	MD3						
1991/07/24	03:33:21.01	2.9	12050336	ONH				0.51965	-0.08	35738851.34
1991/07/24	03:33:21.01	2.9	12050336	PNH						
1991/07/24	03:33:21.01	2.9	12050336	DNH	0.58808	-0.2	35738851.20	0.53016	-0.22	35738851.59
1991/07/24	03:33:21.01	2.9	12050336	WNH						
1991/07/24	03:33:21.01	2.9	12050336	WFM						
1991/07/24	03:33:21.01	2.9	12050336	GLO	0.57034	0.06	35738851.27			
1991/07/24	03:33:21.01	2.9	12050336	WES	0.60697	-0.04	35738851.08			
1991/07/24	03:33:21.01	2.9	12050336	IVT	0.64461	-0.08	35738850.66			
1991/07/24	03:33:21.01	2.9	12050336	BNH						
1991/07/24	03:33:21.01	2.9	12050336	UXB						
1991/07/24	03:33:21.01	2.9	12050336	MD2						
1991/07/24	03:33:21.01	2.9	12050336	MD3						
1990/08/27	06:39:11.38	2.6	02390641	ONH	0.86839	-0.02	64326100.01			
1990/08/27	06:39:11.38	2.6	02390641	PNH	0.86068	0.08	64326101.28	0.50974	0.12	64326101.90
1990/08/27	06:39:11.38	2.6	02390641	DNH						
1990/08/27	06:39:11.38	2.6	02390641	WNH	0.52505	0.04	64326099.40			
1990/08/27	06:39:11.38	2.6	02390641	WFM						
1990/08/27	06:39:11.38	2.6	02390641	GLO						
1990/08/27	06:39:11.38	2.6	02390641	WES	0.55533	-0.02	64326100.70			
1990/08/27	06:39:11.38	2.6	02390641	IVT				0.52332	-0.12	64326101.44
1990/08/27	06:39:11.38	2.6	02390641	BNH						
1990/08/27	06:39:11.38	2.6	02390641	UXB						
1990/08/27	06:39:11.38	2.6	02390641	MD2						
1992/10/06	17:05:49.73	2.9	22801708	ONH				0.53429	0.24	-2325897.42
1992/10/06	17:05:49.73	2.9	22801708	PNH						
1992/10/06	17:05:49.73	2.9	22801708	DNH	0.74022	0.02	-2325897.44	0.89802	-0.26	-2325897.45
1992/10/06	17:05:49.73	2.9	22801708	WNH	0.69009	-0.14	-2325897.48	0.67154	0	-2325897.50
1992/10/06	17:05:49.73	2.9	22801708	WFM	0.88772	0.02	-2325897.44	0.73935	-0.36	-2325897.42
1992/10/06	17:05:49.73	2.9	22801708	GLO	0.8998	-0.08	-2325897.45	0.79179	-0.36	-2325897.44
1992/10/06	17:05:49.73	2.9	22801708	WES	0.80322	-0.12	-2325897.54	0.89074	-0.7	-2325897.52
1992/10/06	17:05:49.73	2.9	22801708	IVT	0.89014	-0.12	-2325897.56	0.89883	-0.12	-2325897.56
1992/10/06	17:05:49.73	2.9	22801708	BNH	0.83519	0.02	-2325897.58	0.83566	-0.2	-2325897.60
1992/10/06	17:05:49.73	2.9	22801708	UXB						
1992/10/06	17:05:49.73	2.9	22801708	MD2				0.88612	0.24	-2325897.52
1992/10/06	15:38:05.46	3.4	22801540	ONH	0.92905	-0.02	-2320633.05	0.65127	0.04	-2320633.04
1992/10/06	15:38:05.46	3.4	22801540	PNH						
1992/10/06	15:38:05.46	3.4	22801540	DNH	0.90389	-0.04	-2320633.04	0.87877	-0.26	-2320633.05
1992/10/06	15:38:05.46	3.4	22801540	WNH	0.62386	0	-2320633.06	0.58948	0.12	-2320633.06

1992/10/06	15:38:05.46	3.4	22801540	WFM	0.92067	-0.36	-2320633.04	0.77428	-0.5	-2320633.04
1992/10/06	15:38:05.46	3.4	22801540	GLO	0.96399	-0.18	-2320633.05	0.87486	-0.4	-2320633.04
1992/10/06	15:38:05.46	3.4	22801540	WES	0.94288	-0.16	-2320633.14	0.85958	-0.7	-2320633.14
1992/10/06	15:38:05.46	3.4	22801540	IVT	0.91076	-0.34	-2320633.14	0.9671	-0.14	-2320633.14
1992/10/06	15:38:05.46	3.4	22801540	BNH	0.84987	-0.08	-2320633.16	0.91229	-0.3	-2320633.16
1992/10/06	15:38:05.46	3.4	22801540	UXB						
1992/10/06	15:38:05.46	3.4	22801540	MD2	0.70205	-2.9	-2320633.14	0.90016	-0.48	-2320633.12

The Header Information is Event Date (YYYY/MM/DD), Origin Time (UTC), Magnitude (Mn). Subdirectory Name is the assigned file name from Weston Observatory that contains waveform data for a specific earthquake. “P Xcorr Value” and “S Xcorr Value” is the cross correlation value of the P-wave and S-wave of the secondary event relative to the master event. “ P Xcorr Diff” and “S Xcorr Diff” is the specific time shift that corresponds to the cross-correlation value listed. The “P Time Diff” and “S Time Diff” is the absolute time difference (in seconds) from the P arrival of the secondary to the master event.

Appendix B: First Motion Selections used in Section 4

Cluster A Composite Focal Mechanism Solution First Motions

Station	Azimuth	Take off Angle	First Motion
ONH	141	125	C
DNH	113	73	D
WNH	12	73	D
HNH	291	73	D
PNH	220	73	D
WFM	176	73	C
GLO	138	73	C
WES	169	73	C
IVT	280	66	D
BNH	10	66	C
TRM	45	66	D
MD2	200	46	C
HBV	314	66	D
MDV	302	66	D
FLE	325	46	C

Mn 3.1 9/17/1990 Focal Mechanism Solution First Motions

Station	Azimuth	Take off Angle	First Motion
ONH	169	109	C
HNH	299	73	D
PNH	235	73	D
DNH	120	73	D
WES	171	73	C
TRM	47	66	D
WNH	12	73	D
WFM	178	73	C
IVT	276	66	D
BNH	10	66	C
GLO	142	73	C

Mn 3.2 3/23/1992 Focal Mechanism Solution First Motions

Station	Azimuth	Take off Angle	First Motion
ONH	141	98.5	C
WNH	28	73	D
HNH	291	73	D
PNH	220	73	D
WFM	173	73	C
IVT	270	73	D
BNH	15	66	C
WES	168	66	C
GLO	143	66	C
TRM	54	66	D
MD2	200	46	C
MIM	47	46	C

The first motions for station WNH accounts for the reversed polarity at WNH and thus lists the initial P-wave first motion as dilatational

Appendix C: Rg/Lg Ratios Per Station used in Section 5

YYYY/MM/DD	HH:MM:SS.xx	-LAT-	-LON-	-DEP-	-ERZ-	Mn	Mc	Station	Station Distance (km)	Rg/Lg per Station
1990/08/27	06:39:11.38	43.31	71.61	7.93	2.6	2.6	2.7	---	---	---
								HNH	70	0.12
								WES	105.4	0.12
								QUA	113.2	0.03
								IVT	119.1	0.21
1990/09/17	23:01:37.64	43.4	71.54	7.25	1.6	3.1	2.5	---	---	---
								HNH	69.5	0.14
								WES	113.9	0.06
								IVT	123.5	0.17
								QUA	124.9	0.05
								BNH	134.5	0.23
								TRM	140.8	0.21
1991/07/24	03:33:21.01	43.32	71.54	9.26		2.9	2.8	---	---	---
								HNH	70.7	0.14
								WES	98.9	0.15
								IVT	127.1	0.10
								TRM	142.9	0.21
								BNH	140.7	0.30
1992/03/23	10:01:50.46	43.53	71.64	4.23	2	3.2	2.7	---	---	---
								HNH	55.4	0.14
								IVT	114	0.07
								BNH	122	0.18
								TRM	138	0.13
								DVT	164.7	0.22
1992/08/26	23:04:48.94	43.25	71.66	7.58	1.5	2.8	2.4	---	---	---
								WES	99.5	0.09
								IVT	117.3	0.08
								BNH	152.9	0.11
								TRM	159.4	0.11
1992/09/09	19:00:51.78	43.34	71.55	6.3	1.1	3.2	2.5	---	---	---
								WES	107.9	0.15
								IVT	123.6	0.11
								BNH	140.7	0.17
1992/10/06	15:38:05.46	43.33	71.56	2.76	2.4	3.4	3	---	---	---
								WES	106.6	0.11
								IVT	122.9	0.09
								BNH	142.4	0.15

YYYY/MM/DD	HH:MM:SS.xx	-LAT-	-LON-	-DEP-	-ERZ-	Mn	Mc	Station	Station Distance (km)	Rg/Lg per Station
1992/10/06	17:05:49.73	43.33	71.54	3.81	1.8	2.9	2.4	---	---	---
								WES	106.7	0.10
								IVT	124	0.12
								BNH	141.8	0.19
								TRM	146.4	0.20
1996/12/12	19:13:42.65	43.67	71.31	12.32		2.5	2.5	---	---	---
								HNH	78.8	0.33
								WES	142.7	0.13
1998/07/07	09:41:42.44	43.21	71.67	0.17		2.1		---	---	---
								HNH	74.2	0.40
								WES	96.1	0.28
								BCX	105.5	0.29
								QUA2	117.8	0.26
								BRY	144.1	0.18
1999/12/10	01:08:51.75	43.24	71.66	8.84	3.4	2.1		---	---	---
								QUA2	121	0.15
2000/10/15	23:49:33.03	43.65	71.39	1.05		2.3		---	---	---
								WES	140.9	0.30
								QUA2	171.5	0.24
2000/12/16	06:05:09.13	43.73	71.51	10.24		2.4		---	---	---
								WES	150.6	0.24
2001/01/03	23:05:29.51	43.65	71.45	20.71		1.6		---	---	---
								HNH	67.6	0.19
2006/10/26	13:03:03.61	43.5	71.63	7.15	0.9	1.8	2	---	---	---
								HNH	57.6	0.09
2009/08/19	20:37:29.83	43.27	71.75	1	1.1	1.6	2.4	---	---	---
								HNH	65.5	0.13
								LBNH	109	0.19
2009/09/09	13:25:06.25	43.65	71.44	13.16		1.9	2.1	---	---	---
								LBNH	76.7	0.23
2009/12/25	20:36:38.27	43.67	71.55	2.57		2.1	2.2	---	---	---
								LBNH	70.6	0.24